Rice University

Department of Earth Science

A Mantle Xenolith Window Into the Grenville Orogeny of Southern Laurentia

by

Hobart Patrick Young

A THESIS SUBMITTED
IN PARTIAL FULFILLMENT OF THE
REQUIREMENTS FOR THE DEGREE OF

Master of Science

APPROVED, THESIS COMMITTEE:

Cin-Ty A. Lee, Associate Professor, Chair, Earth Science

Rajdeep Dasgupta

Rajdeep Dasgupta, Assistant Professor, Earth Science

Richard G Gordon

Richard Gordon, W.M. Keck Professor of Geophysics, Earth Science

HOUSTON, TX
FEBRUARY 2009

Abstract

A mantle xenolith window into the Grenville orogeny of southern Laurentia

by

Hobart Patrick Young

The nature of the lithospheric mantle beneath orogenic belts is incompletely understood due to the paucity of mantle xenolith-bearing basaltic magmas in such regions. One such place where we are afforded the opportunity to study the deep lithosphere beneath an orogenic belt is in central Texas, United States. Mantle xenoliths occur in Late Cretaceous alkali magmas erupted through the remnants of the Appalachian-Ouachita structural belt, Here, we show that geochemical signatures in the form of enrichments in fluid-mobile trace elements (e.g., La) relative to fluid-immobile trace elements (e.g., Nb) are preserved in these xenoliths. We interpret these signatures to represent metasomatism by subduction-related fluids, which implies that the mantle xenoliths represent fragments of continental lithospheric mantle that served as the upper plate during a convergent episode. These observations suggest that some of the original continental lithosphere was preserved beneath the orogenic belt during collision and did not undergo wholesale delamination.

Acknowledgements

Peter Luffi, post-doctorate researcher, Rice University Earth Science

Table of Contents

List of Figures and Tables

A mantle xenolith window into the Grenville orogeny of southern Laurentia

H.P. Young
Department of Earth Science, Rice University, Houston, TX 77005

ABSTRACT:

The nature of the lithospheric mantle beneath orogenic belts is incompletely understood due to the paucity of mantle xenolith-bearing basaltic magmas in such regions. One such place where we are afforded the opportunity to study the deep lithosphere beneath an orogenic belt is in central Texas, United States. Mantle xenoliths occur in Late Cretaceous alkali basaltic magmas erupted through the remnants of the Appalachian-Ouachita structural belt, which represents the former suture of a continent-continent collision. Here, we show that geochemical signatures in the form of enrichments in fluid-mobile trace elements (e.g., La) relative to fluid-immobile trace elements (e.g., Nb) are preserved in these mantle xenoliths. We interpret these signatures to represent metasomatism by subduction-related fluids, which implies that the mantle xenoliths represent fragments of continental lithospheric mantle that served as the upper plate during a convergent episode. These xenoliths may thus represent fragments of the original Proterozoic North American lithosphere, upon which accretionary and collisional processes were superimposed during the continent-continent collisions associated with the Grenville orogeny and subsequent orogenies. These observations suggest that some of the original continental lithosphere was preserved beneath the orogenic belt during continent-continent collision and did not undergo wholesale removal or delamination.

1. INTRODUCTION

Understanding how and when sub-continental lithospheric mantle (SCLM) and the overlying continental crust are generated and then isolated from the convecting mantle is an important problem in the Earth Sciences. The growth and stabilization of continents has long been thought to be related to convergent margins. For example, along convergent margins, subducting oceanic lithosphere drives juvenile arc magmatism while relative plate motions accrete island arc material to the continental margins (Jordan, 1978; Kelemen, 1995; Kelemen et

al., 1993; Lee et al., 2007b; Ringwood, 1975; Rudnick, 1995). However, convergent margins also appear to be regions where large scale convective removal (e.g, "delamination") of the SCLM is thought to occur, as is often depicted in cartoons or invoked to drive post-orogenic magmatism, uplift, and recycling of MgO rich cumulates (Bird, 1979; Houseman et al., 1981; Kay and Kay, 1993; Rudnick, 1995). Such destruction competes with the arc-accretion processes that lead to stable, thick and buoyant cratons.

Understanding the extent of lithospheric mantle recycling during an orogeny is thus of particular interest. Is the SCLM delaminated completely along a lower crustal decollement and replaced with basaltic melts ("underplating") or asthenospheric mantle? Alternatively, is it only partially removed or not at all removed? In essence, our goal is to assess how much of the SCLM can survive a continent-continent collision or a major accretionary episode. These questions can only be answered by examining the nature of the deep lithospheric mantle beneath ancient orogenic belts. Our approach is to use mantle xenoliths as windows into the deep lithosphere, but xenolith-bearing magmas are generally rare in stabilized orogens. One place where an ancient (Mesoproterozoic) orogenic belt is intruded by recent (Late Cretaceous) xenolith-bearing basaltic magmas is along the southeastern margin of the Laurentian craton in west-central Texas, USA. This Mesoproterozoic orogenic belt, which is well exposed in northeastern Laurentia and the Llano uplift, and associated with the greater Grenville orogeny, has a tectonic history that is similar in nature to Phanerozoic orogens and can be qualitatively explained in terms of modern day accretionary processes (Mosher et al., 2008). Here, we present new geochemical data on these mantle xenoliths in order to better understand the relationship between the SCLM and the overlying crustal basement and tectonic history. We then integrate the geochemical data from the mantle xenoliths with geologic studies of the crustal basement as well as geophysical (seismic, gravity, and magnetic) studies of the deep crust and lithosphere.

2. GEOLOGIC HISTORY OF THE LAURENTIAN MARGIN

We begin with a brief overview of the geologic history of the southeast Laurentian margin as is relevant to our study site in west-central Texas. The apparent similarities between the northern Appalachian mountains and their European, Caledonian counterparts were the early observational basis for the theory of continental drift (Bullard, 1965; Wegener, 2001). The northern Gulf of Mexico and Ouachita mountains of Texas, Oklahoma, and Arkansas have a geologic history similar to the Appalachian system to the northeast (King, 1975). In brief, the eastern margin of Laurentia records two distinct Wilson cycles (Keller and Hatcher, 1999), the first culminating in the mid- to late Proterozoic Grenville orogeny, the second in the Paleozoic Alleghenian orogeny.

Grenville orogeny (Proterozoic)

The Grenville orogeny, occurring ~1 Ga, is recognized on both sides of the Atlantic Ocean as well as in Australia and Antarctica, and is associated with the formation of the supercontinent Rodinia (e.g.Keller and Hatcher, 1999; Torsvik et al., 1996). It has been extensively studied in the Eastern United States and Canada where basement rocks of Grenville age outcrop in the Blue Ridge Province and the Eastern Valley and Ridge Province of the Appalachian mountains (e.g. Keller and Hatcher, 1999). The location of this province, which is the eastern extent of Proterozoic outcrop in Laurentia, is delimited in Figure 1 by the thick yellow and black lines. In southern Laurentia, Proterozoic rocks are exposed in the Llano uplift of central Texas and also near the Grenville front in west Texas (Figure 1). The Grenville front is recognized from a magnetic and gravity anomaly and has been seismically imaged in Ohio where it is interpreted to be an intracratonic, foreland fold and thrust belt and the western extent of Grenvillian deformation (Culotta et al., 1990). The front separates undeformed granitic basement to the northwest from gneisses and metasedimentary rocks to the southeast (Mosher, 1998). The vast majority of the mid-continent to the northwest of the Grenville front (the Great Plains) is composed of Paleoproterozoic granitic and volcanic basement rocks (Hoffman, 1988; Van

Schmus, 1996) emplaced under orogenic tectonic conditions between 1800 Ma and ~1600 Ma (Bickford et al., 2000). Another suite of granitoids intruded Paleoproterozoic crust from ~1400 Ma under "anorogenic" conditions (Goodge and Vervoort, 2006).

The main tectonic features in the Grenville province are continental arc magmatism and intense collisional deformation. A seismic study of the Grenville province in Ohio revealed a west-dipping suture (Fig. 1), which is evidence for subduction beneath the Laurentian craton (Culotta et al., 1990). In addition, the oldest terrane of the Llano uplift - the 1232 Ma Valley Spring gneiss - is interpreted to be a Laurentian continental arc terrane because Laurentian zircons are contained in trench sediments (Mosher, 1998). The tectonic features seen in Quebec also indicate that the Laurentian craton was intruded by continental arc magmatism prior to collisional orogenesis (Rivers et al., 1993). These observations place a NE-SW striking convergent-destructive plate boundary along the southern and eastern margin of Laurentia, recording a progression from continental arc magmatism to arc-continent collision and finally continent-continent collision (Mosher, 1998; Mosher et al., 2008). The process of plate destruction beneath North America and production of new continental crust culminated in the suturing of Laurentia to an unknown continent 1 Ga to form the supercontinent of Rodinia (Mosher, 1998). Post-orogenic or anorogenic 1.1-1.0 Ga "A-type" granites also occur in the Grenville province (Mosher, 1998; Walker, 1992). Exposure of medium temperature eclogites in Llano and deep crustal exhumation in Quebec (Rivers et al., 1993) suggest exhumation of half the thickness of the orogen. Mosher et al. suggested lithospheric delamination may have driven this uplift (2008).

Alleghanian orogeny (Paleozoic)

Between 1 Ga and 300 Ma, the continents split apart and came together again in a classic Wilson cycle. During this cycle, however, the oceans closed on their southern or "African" edge (in the case of the Rheic) or in a far-removed intraocean setting, analogous to the present day western Pacific (in the case of the Iapetus) (Pickering, 1989; Pickering and Smith, 1995). North America then grew by accretion of microcontinents and volcanic arcs (Keller and Hatcher, 1999; Rankin, 1994) (see overview in Hatcher et al. (1989)). The Late Paleozoic orogeny

culminated in what is known as the Alleghenian orogeny, which was another continent-continent collision, this time between Laurentia and Gondwana, resulting in the supercontinent Pangea. This orogeny, however, involved more thin-skinned allochthonous tectonics and more limited metamorphism along much of the Laurentian belt compared to the Grenvillian orogeny (Keller and Hatcher, 1999). Based on the high burial depths of the Laurentian margin beneath the exotic Avalon terrane, it is likely that Laurentia served as the underlying plate along much of the suture during the Paleozoic orogenies (Keller and Hatcher, 1999). Hence, the geometry of the Alleghenian orogeny differed from the Grenvillian orogeny, wherein Laurentia was the destructive margin and served as the over-riding plate prior to continent-continent collision. The final suture of Gondwana with Laurentia is recognized in both seismic reflection and magnetic anomaly data, marking a major crustal boundary as can be seen in Fig. 1 (Buffler and Thomas, 1994). The suture appears to be east-dipping, providing additional evidence that the Laurentian margin served as the under-riding plate and Gondwana served as the upper plate (Buffler and Thomas, 1994). A number of African terranes (Suwanee) occur south of the suture. Accretion of exotic terranes to the passive margin caused significant compression of the Paleozoic basins in the central Appalachians, but the consensus seems to be that no continental arc formed along the southern margin of Laurentia in Paleozoic times and hence subduction was not proximal to Laurentia (Keller and Hatcher, 1999).

Opening of the Gulf of Mexico

The final episode of opening to form the modern Gulf of Mexico and Atlantic Ocean began in the Jurassic (continuing today in the Atlantic and ending in the Late Jurassic for the Gulf). Opening of the Gulf of Mexico resulted in significant thinning and attenuation of the lithosphere along the Texas – Louisiana gulf coast (Dunbar and Sawyer, 1987). This rifting may have removed a large area of Proterozoic basement from the midcontinent region (Thomas, 1991; Thomas and Astini, 1996), which further raises questions about the integrity of the deep lithosphere beneath the Laurentian margin through time.

Present day structural remnants of the orogenies

The trend of exposed and deeply exhumed Appalachian structures and Precambrian basement dives beneath the southern Gulf Plain (see Fig. 1). Except in the Llano uplift, Precambrian lithosphere is known in the Gulf Coast region only through drill cores which penetrate isolated uplifts. The eastern margin of the United States and Canada has been the focus of regional geophysical studies to decipher lower crustal structure (Culotta et al., 1992; Culotta et al., 1990; Keller et al., 1989; Mickus and Keller, 1992). Where the Paleozoic structural belt is buried, its location has long been inferred to follow the trend of a steep change in potential field (Flawn, 1961). Figure 1 also shows the outline of the positive section of this gravity anomaly, which is interpreted to have been a suture between Laurentia and Gondwana during the Paleozoic and delimits the core of the Paleozoic Ouachita – Appalachian structural belt (Flawn, 1961).

3. GEOLOGIC SETTING OF THE STUDY AREA

Lithospheric mantle xenoliths (spinel lherzolites) were collected from the Vulcan open pit quarry in the town of Knippa at 29.29N 99.65W, located in Uvalde county, TX (Figure 1). The xenoliths are hosted in a fine-grained, olivine nephenilite. There are also fine to coarse-grained alkali basalts, olivine nephelinites, nepheline basanites, and phonolites in the area (Miggins, 2004). The basaltic magmas are associated with a series of Late Cretaceous basalts erupted through Cretaceous shallow marine sediments, forming mostly hypabyssal laccoliths, plugs, sills, and dikes along with accumulations of ash and tuff that settled in water (Ewing and Caran, 1982). The volcanoes appear to have intruded through the buried Paleozoic structural belt (delimited by the trend of the gravity anomaly), where Mesozoic sediments overlie Proterozoic Laurentian basement (Flawn, 1961). Miggins (2004) dates the eruption of these basalts between 80-82 Ma based on $^{40}Ar/^{39}Ar$ chronology.

The Knippa basalts appear to be related to a much larger volcanic province that stretches from south-central Texas east through Oklahoma and Arkansas. For example, Lonsdale (1927)

described basaltic volcanic rocks near Austin, which is northeast of Knippa. Late Mesozoic alkali igneous activity also occurs along the Ouachita belt in Arkansas and Oklahoma (Byerly, 1991, see Fig.1). Spencer (1969) recognized that these widely spaced volcanic provinces were probably related temporally and tectonically. He named this volcanic province the "Balcones Igneous Province" because the trend of the volcanic rocks and hypabyssal intrusive laccoliths and plugs followed the buried Paleozoic Ouachita structural belt, which in southwest Texas follows the Balcones escarpment. Magnetic surveys have since confirmed how extensive the Balcones Igneous Province is (Ewing and Caran, 1982). In Figure 1 (inset), the locations of magmatic intrusions are reproduced from Ewing and Caran (1982). The locations of the Balcones and Luling faults are also shown. The broad zone of Cretaceous igneous activity in Texas is roughly bounded by the Balcones and Luling fault zones and also lies inside the trend of the regional positive gravity anomaly. Ewing and Caran (1982) attributed the trend of volcanic activity to Miocene and younger style faulting, which generated the Balcones escarpment. However, given the Cretaceous ages of the volcanic province, it is more likely that the trends of both the Cretaceous igneous activity and the subsidence-related Balcones and Luling fault zones are controlled by the trend of the older and structurally more significant, Ouachita system as suggested by Spencer (1969). In any case, the exact origin of these basalts remains unclear and is a subject for further study. It has been suggested that loading of the Gulf with sediment would concentrate flexure of the lithosphere near a structural hinge such as the Ouachita structural belt (Miser, 1934), but flexure alone may not be sufficient to cause melting.

The Knippa volcanics are centered within the Balcones Igneous Province, hence the Knippa xenoliths should provide insight into the nature of the lithosphere beneath the ancient Laurentian margin. We will use the xenoliths and their geographic location to determine the extent and location of subsurface features in Texas, including the location of the Grenville province and a possible hinge between Proterozoic craton and Phanerozoic accreted terranes.

4. XENOLITH PETROGRAPHY:

The xenoliths are clinopyroxene-poor lherzolites and harzburgites, containing variable proportions of olivine (ol), orthopyroxene (opx), clinopyoxene (cpx), and spinel (sp). The xenoliths occur as angular fragments within the basalt. Limited reaction between the host basalt and the xenoliths can be seen in the form of brownish 1 mm thick rims around the mantle xenoliths. The unreacted interiors of these xenoliths, however, still retain the original olivine-green color characteristic of unreacted peridotites.

Nine xenoliths were analyzed in this paper. Modal abundances are difficult to calculate accurately because of the small size of the xenoliths (0.75 – 2 cm in diameter) and their coarse-grained nature (>1mm). Modes were estimated by two methods. The first approach was point counting. However, many cpx grains were much smaller than the average grain size of the xenoliths, and this resulted in either an over-estimate or under-estimate of cpx mode. To better assess cpx mode, we estimated the areal proportion of cpx in thin section (areal estimates and point counts of ol and opx modes were similar). The resulting mineral modes are 70 – 72 % ol, 21 – 25 % opx, 3 – 8% cpx, and ~2% sp for samples 02A, 02F, 05A, 05B, 11B, and 15B. These modal mineralogies are similar to the dominant types of residual peridotite xenoliths worldwide. Two samples (01A and 08A) are opx-rich and have <3% cpx and are classified as refractory harzburgites. Sample 06E appears depleted in opx (~10%), though in every other respect it is similar to the other lherzolites, so this is attributed to poor statistical sampling.

Texturally, the xenolith grains are coarse, equigranular to slightly tabular and have many well-developed triple junctions. Sample 08A is the only sample to show textural evidence for deformation: alignment of spinels and orthopyroxenes defines a weak foliation and spinels occur as slightly elongated blebs. Clinopyroxenes of varying texture occur. Most cpx grains are heavily "corroded" with spongy or turbid textures, which we interpret to be due to flash-heating and decompression during ascent in the host basalt. Some clinopyroxenes have only a spongy rim, and this rim is diffuse when sharing an edge with orthopyroxene. Only for the occasional large clinopyroxenes (~1.5 mm) were cores clear and without any distinctive turbid textures.

Orthopyroxenes have well defined edges and occur in clusters. They are light green in plain light, and cleavage fractures are visible in plane polarized light. The olivine is equigranular to tabular shaped and coarse-grained (up to 3 mm). The olivines are sometimes cut by thin serpentinized veins, which are associated with post-emplacement weathering.

5. METHODS

Xenoliths were chosen for size and freshness, cut out of the host basalt, and made into 200 micron doubly polished thick sections for analytical work (as well as 30 micron doubly polished thin sections for petrographic analysis). Samples were analyzed for major and trace elements using laser ablation inductively coupled plasma (LA-ICP-MS) mass spectrometry using a ThermoFinnigan Element 2 ICP-MS at Rice University. Minerals in the thick sections were ablated using a 213 nm wavelength NewWave laser, pulsing at 10 Hz with a 55 micron spot size at 20 J/cm^2. Minerals analyzed were selected and targeted with the laser microscope viewfinder to avoid grain boundaries, inclusions, and cracks. We performed one medium (major elements) and one low mass resolution (trace elements) analysis on the core of each mineral analyzed. For analysis, 10 to 12 cycles of background signal were recorded prior to firing the laser and 30 to 40 cycles of signal were recorded during ablation. Drift effects and decay of the signal were corrected for using ^{25}Mg as an internal standard (Longerich et al., 1996). Three external basalt standards BHVO2g, BIR1g, and BCR2g were simultaneously used for concentration calibrations. The ICP-MS and laser gases (Helium) were tuned before analysis of standards and samples to attain a sensitivity of >600,000 cps for 15 ppm La in BHVO2g (10 Hz, 55 micron spot size). Major element concentrations were estimated from medium resolution measurements by assuming all major and minor elements (Si, Mg, Ca, Fe, Mn, Ti, Na, K, Al) were oxides and that the oxides summed up to 100 %. The resulting Mg content was then used as the internal standard for converting low mass resolution trace element signals to concentrations.

Fig. 2 is a typical example of the raw data. Sufficiently constant signals were attained for every element except Rb, Cs, and Ba throughout the study. For example, in Fig 2a, it can be

seen that the signal for Cs is orders of magnitude higher in the first half of ablation interval. Condie et al. (2004) have shown that large ion lithophile elements tend to accumulate along grain boundaries and in microcracks. We assume this is the cause for variable intensities of Cs, Rb, and Ba as opposed to surface contamination associated with sample preparation. Indeed, these occasional pulses of Cs, Rb and Ba are most evident in those cpx grains which have a "spongy" texture and thus may be related to micro-cracks or inclusions. No anomalous pulses were observed for Th, U, or Pb, which are often thought to behave similarly to Cs, Rb and Ba.

Signal quality was ultimately assessed by examining time-resolved plots of normalized elemental intensities. It can be seen in Fig 2b that internally normalized ratios are constant and do not cross each other, indicating homogeneity for most elements. In the case of Cs, Rb, and Ba, their normalized intensities are not constant and therefore cross other normalized elements. We eliminated that part of the signal that was not parallel to the other elements. Nb and Zr in spinels suffered from CrAr isobaric interferences (Eggins et al., 1998) and were therefore discarded. Nb and Zr contents in peridotitic spinels are generally low and do not contribute a significant budget to the whole rock Nb and Zr contents.

6. RESULTS

In Table 1, we present the modes, major oxide weight percents and trace element concentrations in ppm for mineral phases in each sample. These values reflect the average of all measurements run on the respective phase for that sample. In Table 2, we report the mineral modes, major oxide weight percents, trace element concentrations in ppm, and calculated equilibration temperatures of the whole rock. Whole-rock compositions were estimated by summing up the mineral compositions according to their estimated proportions. In the case of 02F and 06E, spinels were too small to be analyzed so the average composition of spinels in the other samples was used to reconstruct the major oxides for the bulk rock. Bulk trace element

reconstructions for 02F and 06E do not take spinel into account at all, however, the total contribution from spinel is negligible in other samples anyway.

Thermobarometry:

Temperatures of equilibration were estimated from Mg-Fe exchange between clinopyroxene and orthopyroxene using the method of Wells (1977) and Brey and Kohler (1990) after normalizing mineral major element oxide compositions to 100 wt. %. For the Brey and Kohler thermobarometer, a reasonable range of pressures for spinel lherzolites (20 – 25 kb) was assumed. Our calculations indicate equilibration temperatures between 860-1142 °C using the Well's thermometer and between 820-1090 °C with the Brey and Kohler thermometer (one sample gives an anomalously low Brey and Kohler temperature of 786 °C) (Table 2). The average temperature of equilibration is 978 °C according to the method of Wells (1977) and 957 °C according to the method of Brey and Kohler (1990). Direct estimate of pressure was not possible because of the lack of appropriate mineral assemblages (e.g., garnet) for barometry.

Crude limits on pressure were determined by using the thermobarometric temperatures and fitting them to model continental geotherms (Figure 3). The present day surface heat flow in the region is ~50 mW/m^2 (Pollack et al., 1993; Woodruff and Foley, 1985), resulting in a depth of ~70 km for the minimum calculated temperature of 786 °C. However, given the large range in temperatures, these xenoliths could have equilibrated at pressures and depths approaching 3 GPa, but due to the lack of garnet in these samples they are unlikely to come from depths greater than ~85 km (Klemme, 2004). If heat flow was appreciably greater in the Cretaceous (70 mW/m^2) then the depth of equilibration could have been as shallow as 40 km although this is unlikely given the passive nature of the margin at that time. We thus conclude that these xenoliths equilibrated at approximately 950 °C and at depths between 70 – 80 km. The xenolith P-Ts appear to be associated with lithosphere that is thinner and warmer than typical Archean cratonic lithosphere, but significantly cooler than Phanerozoic lithospheric mantle, such as in the Basin and Range Province.

Major and minor element chemistry:

Mineral chemistries show similarities to continental lithospheric mantle samples. For example, Mg#s (molar Mg/(Mg+Fe)) of olivine, clinopyroxene, orthopyroxene, and the whole rock range from 0.89 - 0.91, .91-.94, .89-.91 and .89-.91, respectively, and are slightly higher than that of primitive mantle olivines (~0.89) but not as high as Archean cratonic mantle olivines (0.91-0.93). Al_2O_3 and Na_2O contents of pyroxenes are low and the Ni contents of olivines are high, which is typical of continental peridotite xenoliths. These high Mg#s, high Ni contents and low Al contents all suggest these minerals derive from refractory peridotites, such as harzburgites and cpx-poor lherzolites though the possibility of some amount of refertilization is not excluded.

Whole-rock compositions, estimated by reconstructing mineral modes and compositions, are also consistent with a refractory origin. Compared to fertile lherzolite, such as model primitive mantle compositions, the Knippa peridotites have high whole-rock MgO and low CaO, Na_2O, and Al_2O_3 (Fig 4(a-c)). Error bars account for variations in estimated modal abundances which far outweigh errors associated with mineral compositions. In a plot of CaO versus MgO (Fig. 3a), the Knippa peridotites fall within the same trend as seen in abyssal peridotites and peridotite xenoliths from Phanerozoic and Proterozoic continental lithosphere. There is no evidence from mineral modes or whole-rock chemistry to indicate that any of these samples are anomalously rich in Si as is seen in some Archean cratonic mantle peridotites. The low Ca, Al, and Na contents and the negative correlation of these oxides with MgO are consistent with the Knippa peridotites representing the residues of previous melt depletion.

Trace Element Chemistry:

Primitive mantle-normalized (McDonough and Sun, 1995) trace element spidergrams for reconstructed whole-rocks are presented in Figure 5a and plotted in order of increasing compatibility in the solid peridotite residue. Included in these whole-rock reconstructions are the trace-element compositions of cpx, opx and ol, but not sp. The modal abundance of sp is small and the concentrations of trace elements in sp are also small, so the effect of spinel on bulk trace element compositions is negligible (Cr is an exception as spinel dominates the whole-rock Cr

budget). In some cases, we were not able to measure the highly incompatible element abundances in olivine (e.g., the light rare earths, LREEs) because they were below detection limits, but the abundances of these elements are so low in olivine that they do not contribute to the bulk rock composition. Thus, for the most part, the whole-rock trace element budget is controlled by opx and cpx.

A key feature of the whole-rock spidergrams is the depletion in moderately incompatible trace elements, such as the heavy rare earth elements (HREEs), relative to primitive mantle. In general, moderately incompatible elements, such as the HREEs, are more resistant to metasomatic disturbances (Canil, 2004; Lee et al., 2007a), hence the HREE depletions likely reflect melt depletion. Indeed, HREE depletion correlates with major element indices of depletion as can be seen by the correlation of Ca versus Lu (Fig. 4d).

Melt depletion, however, should result in positively sloping REE spidergrams (e.g., LREE depletion relative to HREEs) due to more efficient extraction of highly incompatible elements. However, "U-shaped" trends are seen, as exemplified by the relative enrichment in LREEs. High La/Sm and Sm/Yb ratios in our samples are reminiscent of metasomatized mantle xenoliths in sub-arc or post-Archean continental settings as well as enriched magmas, such as arc magmas (Fig. 6). They do not match the highly LREE-depleted signatures of oceanic abyssal peridotites (Niu, 1997), nor do they match typical mid-ocean ridge basalts, which are also depleted in LREEs relative to HREEs. Carbonatite-metasomatized xenoliths (Yaxley et al., 1991) have much steeper LREE enrichment patterns than the Knippa peridotites. These observations suggest that these xenoliths were cryptically re-enriched in incompatible trace elements after the melt depletion event that gave rise to their refractory major element compositions.

We also examined the high field strength element abundances (HFSEs): Nb, Ta, Zr, Hf and Ti. It is generally thought that depletions in these elements relative to the REE partner that exhibits the most similar bulk partition coefficients during anhydrous peridotite melting is a sign of hydrous fluid metasomatism because the HFSEs are considered much less fluid-mobile than the REEs. Relative depletions in these elements occur in our cpx grains, but these relative depletions alone in cpx do not by themselves imply metasomatism by HFSE-depleted fluids/melts

as such depletions commonly occur in cpx grains from other mantle xenolith suites (much of the whole-rock HFSE budget is also housed in opx). Thus, it is often the case that whole-rocks show little HFSE depletion even though cpx's are HFSE-depleted. However, this is not the case in the Knippa samples. In all but two of the most refractory samples (01A and 08A), the reconstructed whole-rock HFSEs show relative depletions. For example, whole-rock Nb and Ta are depleted relative to La, Zr and Hf are depleted relative to Sm, and Ti is depleted relative to Eu. These HFSE depletions are typically found only in arc magmas or in mantle xenoliths that have been metasomatized by fluids (Kelemen et al., 1993). Because of the low fluid solubilities of HFSEs compared to the REEs, fluid metasomatism typically yields HFSE-depletion signatures whereas no HFSE anomalies are generated during silicate melt metasomatism.

Large ion lithophile elements (LILEs), such as Ba, Cs, and Rb, were more difficult to reconstruct because of their low concentrations in silicate minerals. We observed enrichments in these elements in some clinopyroxenes. Fig. 7 shows the PM normalized concentrations of trace elements in clinopyroxenes from sample 05A. As discussed in the petrography section above, two textures of clinopyroxenes exist, the more common being the "turbid" cpx. Turbid clinopyroxenes show variable but high concentrations of Cs, Rb, and Ba. The clear-cored cpx of 05A (two shots (a) and (b)) have much lower concentrations of LILE's. In addition, we also found that the rims of clinopyroxenes showed enrichment in these elements compared to the core, thus it is not clear what fraction of these enrichments are due to ancient fluid metasomatic events or more recent disturbances associated with the magmatic precursor to the host magma.

Assessing trace-element equilibrium:

An important question regarding trace-element compositions of mantle xenoliths is whether the compositions are actually representative of the mantle or if they represent recent perturbations associated with contamination by the host magma. One way to address this problem is to assess whether the mineral chemistries have equilibrated. If the mineral chemistries have been recently disturbed, they should be out of equilibrium. Lee et al. (2007a) and Agranier and Lee (2007) showed by extension of lattice strain theory to mineral-mineral

element partitioning, that when equilibrium exists between mantle pyroxenes, there is a nearly log linear variation in the ratio C(opx)/C(cpx) with increasing ionic radius of the lanthanide series. Samples that were contaminated or recently metasomatized show deviations from this log-linear trend. Fig. 8 demonstrates that there is for the most part a log linear variation in the concentrations of REEs in orthopyroxene over clinopyroxene for the Knippa peridotites. These observations indicate that, at least for the REEs, equilibrium has been achieved and the reconstructed whole-rock REE patterns are probably representative of the mantle. While we have not been able to do the same for the HFSEs, we assume that the high degree of equilibrium seen in the REEs hints that the HFSEs are also in equilibrium.

7. DISCUSSION

The Knippa xenoliths have whole-rock and mineral chemistries characteristic of the sub-continental lithospheric mantle (SCLM). Equilibration temperatures of 800-1100 °C are too cool to be associated with hot plumes or asthenospheric mantle. Interpolating from model geotherms, these temperatures suggest that the xenoliths derived from depths of ~70-80 km, which implies that the base of the thermal boundary layer beneath Knippa could have been as thick as ~100 km (taking ~1300 °C to represent the temperature at the base of the thermal boundary layer). The enrichments of the LREEs and LILEs over middle and heavy REEs is inconsistent with fertile asthenosphere or oceanic mantle origin and instead require that these peridotites were cryptically metasomatized sometime after they were formed by melt depletion (as in Fig 6). Of key importance are the depletions in HFSEs relative to the REEs; these negative HFSE anomalies suggest the involvement of fluids during metasomatism and are often taken to imply an arc origin (Hofmann, 1988; Kelemen et al., 1993; Ryerson and Watson, 1987). Similar features have been seen in mantle xenoliths from the Sierra Nevada (Lee, 2005) and Canadian Cordillera (Peslier et al., 2002).

We envision the origin of the geochemical signatures as follows. Melt was originally extracted from these peridotites, resulting in low Ca, Al and HREE contents and high Mg# and MgO. Based on the depletions in Ca, Al and HREE contents with respect to an assumed fertile mantle starting composition, we estimate that these peridotites had ~15-20 % melt extracted (using experimental compositions of Walter (Walter et al., 2003; Walter et al., 1995) and parameterizations from pMELTs (Ghiorso and Sack, 1995)). Such a melting event should generate much more depletion in LREEs and HFSEs relative to the HREEs (Fig. 5b). Thus, after the original melting event, small degrees of fluids or melts had to be added into the residual peridotite. In Fig. 5b, we demonstrate the different effects of mixing melt-depleted peridotites with melts having no arc signature (MORB or OIB) and melts/fluids with a HFSE depletion. For the REEs, it can be seen that only small amounts of melt/fluid addition (0.5-2.0 %) is needed to match the LREE enrichment levels (note that HREEs remain unaffected). However, only the addition of HFSE-poor melts/fluids can generate the negative HFSE anomalies in the Knippa peridotites. The Knippa peridotites most likely represent fragments of SCLM that were metasomatized by arc-like fluids. In contrast, the relatively flat REE patterns and lack of pronounced HFSE anomalies in samples 01A and 08A suggest metasomatism by silicate melts rather than fluids. These samples were metasomatized a second time (by silicate melts), which overprinted an original arc signature. Alternatively, these samples were never metasomatized by fluids.

The metasomatic history of the lithospheric mantle beneath Knippa appears to be heterogeneous. However, what is important here is that many of the xenolith samples preserve an arc or subduction signature, begging the question of when this signature was imparted. The late Cretaceous (~80 Ma) eruption of the host lava precludes the arc signature from being related to low angle subduction of the Farallon plate beneath North America, which happened between ~74-40 Ma. There has also been no subduction along the Gulf of Mexico for the last 300 My. The only times known to have subduction were just before the Proterozoic Grenville (1000 My) and Paleozoic Alleghenian (300 My) orogenies. However, as discussed in the geologic background section, the Texas Laurentian margin was a destructive margin only during the pre-Grenvillian

times and not during pre-Alleghenian times (Hatcher, 1989). If so, the fluid geochemical signatures could represent subduction imprints associated with closing of an ocean basin that culminated in the Grenvillian orogeny. This would imply that the Knippa xenoliths represent original Proterozoic Laurentian lithospheric mantle. This interpretation is consistent with isotopic studies done on peridotite xenoliths from the Prairie Creek lamproiites in Arkansas, which are contemporary and most likely tectonically related to the Knippa basalts and the Balcones Igneous Province (Lambert et al., 1995). Indeed, the Prairie Creek lamproiites are situated near the trend of the positive Bouguer gravity anomaly and the inferred edge of the North American craton. The Re-Os and Sm-Nd isotopic signatures of the lamproites and mantle xenoliths from Prairie Creek point to a lithospheric mantle with a Proterozoic separation age of 1.2 Ga (Lambert et al., 1995). For comparison, the age of the overlying igneous crust is ~1.4 Ga (Nelson and Depaolo, 1985).

Collectively, these observations suggest that growth of the Laurentian margin occurred just prior to the Grenville orogeny, perhaps associated with the accretion of arc terranes associated with closing of an ocean basin. Closing of the ocean basin culminated in the Grenville orogeny, continent-continent collision at 1.0 Ga. The details of what happened to the newly accreted Laurentian margin during the Grenville orogeny in southern Laurentia are still debated. Many have suggested that after continent-continent collisions, lithospheric mantle in general will be delaminated (Bird, 1979; Corrigan and Hanmer, 1997; Davies and Vonblanckenburg, 1995; Houseman et al., 1981; Turner et al., 1996). However, the preservation of subduction zone geochemistry in the mantle beneath Grenville age rocks in southern Laurentia suggests that large fractions of the original mantle root was not delaminated during the Grenville or Alleghenian orogenies and may have instead been preserved for over 1 billion years.

This conclusion seems somewhat surprising at face value because the Knippa xenoliths are not as refractory as many Archean cratonic mantle peridotites, whose densities are consequently so low that it is difficult to destabilize them from buoyancy considerations alone. The Mg#s of the Knippa xenoliths are similar to other post-Archean lithospheric mantle, hence their chemical buoyancies are not likely to be as high as typical cratonic mantle peridotites. The fact that much of the original SCLM beneath the southern margin of Laurentia is still preserved

suggests that density alone is not controlling the long-term preservation of continental lithospheric mantle. One possibility is rheology. The viscosity of the Laurentian margin could have been high either because the lithospheric mantle had been dehydrated during partial melting or the lithospheric mantle had already stabilized, cooled and strengthened (Hirth and Kohlstedt, 1996). The Knippa xenoliths show subduction-related signatures, which implies that the nominally anhydrous minerals (olivine and pyroxenes) may have been rehydrated, and if so, one would expect much of the lithospheric mantle to have been weakened and possibly removed. The original lithosphere thickness along the southern Laurentian margin could have been at least ~150 km thick based on the presence of diamonds in the Prairie Creek lamproiite in Arkansas. The fact that the present lithosphere thickness beneath Knippa is <80 km, suggests that the lower half may indeed have been progressively removed. The upper part of the lithosphere, being colder, may have escaped delamination because it was just too cold to deform. Regardless of the details of our interpretations, what is clear is that even in large continent-continent collisions, much of the pre-orogenic continental lithospheric mantle remains. This leads us to speculate that continental lithospheric mantle, however it is formed, is relatively resistant to being recycled completely into the mantle, but the mechanism of preserving such lithosphere still remains elusive.

8. CONCLUSIONS

A. Mantle xenoliths erupted through the lithosphere along the Texas coast are characteristic of continental lithosphere and show strong evidence for high field strength element-poor metasomatism, suggesting a relationship with arc or subduction-related fluids.

B. The origin of these arc-signatures is most likely a pre-Grenville subduction zone and mantle wedge.

C. Despite voluminous "post-orogenic" alkalic granitic plutonism all through the Grenville province of Laurentia, two episodes of supercontinent rifting and tectonic thinning, and over 1Ga Earth history, the original metasomatized mantle wedge of the Grenville event is largely preserved beneath the crust.

Agranier, A., and Lee, C.T.A., 2007, Quantifying trace element disequilibria in mantle xenoliths and abyssal peridotites: Earth and Planetary Science Letters, v. 257, p. 290-298.

Bickford, M.E., Soegaard, K., Nielsen, K.C., and McLelland, J.M., 2000, Geology and geochronology of Grenville-age rocks in the Van Horn and Franklin Mountains area, west Texas: Implications for the tectonic evolution of Laurentia during the Grenville: Geological Society of America Bulletin, v. 112, p. 1134-1148.

Bird, P., 1979, Continental delamination and the colorado plateau: Journal of Geophysical Research, v. 84, p. 7561-7571.

Brey, G.P., and Kohler, T., 1990, Geothermobarometry in 4-phase lherzolites. 2. New thermobarometers, and practical assessment of existing thermobarometers, Journal of Petrology, v. 31, p. 1353-1378.

Buffler, R.T., and Thomas, W.A., 1994, Crustal structure and evolution of the southeastern margin of North America and the Gulf of Mexico Basin, *in* Speed, R.C., ed.: Boulder, Geological Society of America.

Bullard, E.C., 1965, Fit of the continents around the Atlantic: Science, v. 148, p. 664-.

Byerly, G.R., 1991, Igneous activity, *in* Salvador, A., The Gulf of Mexico Basin The Geology of North America: Geol. Soc. America, v. J, p. 91-108.

Canil, D., 2004, Mildly incompatible elements in peridotites and the origins of mantle lithosphere: Lithos, v. 77, p. 375-393.

Condie, K.C., Cox, J., O'Reilly, S.Y., Griffin, W.L., and Kerrich, R., 2004, Distribution of high field strength and rare earth elements in mantle and lower crustal xenoliths from the Southwestern United States: The role of grain-boundary phases: Geochimica Et Cosmochimica Acta, v. 68, p. 3919-3942.

Corrigan, D., and Hanmer, S., 1997, Anorthosites and related granitoids in the Grenville orogen: A product of convective thinning of the lithosphere?: Geology, v. 25, p. 61-64.

Culotta, R., Latham, T., Sydow, M., Oliver, J., Brown, L., and Kaufman, S., 1992, Deep-Structure of the Texas Gulf passive margin and its Ouachita-Precambrian basement - results of the COCORP San-Marcos Arch survey: AAPG Bulletin-American Association of Petroleum Geologists, v. 76, p. 270-283.

Culotta, R.C., Pratt, T., and Oliver, J., 1990, A tale of 2 sutures - COCORP's deep seismic surveys of the Grenville Province in the Eastern United-States Midcontinent: Geology, v. 18, p. 646-649.

Davies, J.H., and Vonblanckenburg, F., 1995, Slab breakoff - a model of lithosphere detachment and its test in the magmatism and deformation of collisional orogens: Earth and Planetary Science Letters, v. 129, p. 85-102.

Dunbar, J.A., and Sawyer, D.S., 1987, Implications of continental-crust extension for plate reconstruction - an example from the Gulf of Mexico: Tectonics, v. 6, p. 739-755.

Eggins, S.M., Rudnick, R.L., and McDonough, W.F., 1998, The composition of peridotites and their minerals: A laser-ablation ICP-MS study: Earth and Planetary Science Letters, v. 154, p. 53-71.

Ewing, T.E., and Caran, S.C., 1982, Late Cretaceous volcanism in South and Central Texas - stratigraphic, structural, and seismic Models: AAPG Bulletin-American Association of Petroleum Geologists, v. 66, p. 1429-1429.

Flawn, P.T., Goldstein, A., King, P.B. and Weaver, C.E., 1961, The Ouachita System: Bureau of Economic Geology, University of Texas, Austin p. 401.

Ghiorso, M.S., and Sack, R.O., 1995, Chemical mass transfer in magmatic processes IV. A revised and internally consistent thermodynamic model for the interpolation and extrapolation

of liquid-solid equilibria in magmatic systems at elevated temperatures and pressures: Contributions to Mineralogy and Petrology, v. 119, p. 197-212.

Goodge, J.W., and Vervoort, J.D., 2006, Origin of Mesoproterozoic A-type granites in Laurentia: Hf isotope evidence: Earth and Planetary Science Letters, v. 243, p. 711-731.

Hatcher, R.D., Jr., 1989, Tectonic synthesis of the U.S. Appalachians, *in* Hatcher, R.D., Jr., Thomas, W.A., and Viele, G.W., eds.: Boulder, Geol. Soc. Am.

Hirth, G., and Kohlstedt, D.L., 1996, Water in the oceanic upper mantle: Implications for rheology, melt extraction and the evolution of the lithosphere: Earth and Planetary Science Letters, v. 144, p. 93-108.

Hoffman, P.F., 1988, United Plates of America, the Birth of a Craton - Early Proterozoic Assembly and Growth of Laurentia: Annual Review of Earth and Planetary Sciences, v. 16, p. 543-603.

Hofmann, A.W., 1988, Chemical Differentiation of the Earth - the Relationship between Mantle, Continental-Crust, and Oceanic-Crust: Earth and Planetary Science Letters, v. 90, p. 297-314.

Houseman, G.A., Mckenzie, D.P., and Molnar, P., 1981, Convective instability of a thickened boundary-layer and its relevance for the thermal evolution of continental convergent belts: Journal of Geophysical Research, v. 86, p. 6115-6132.

Jordan, T.H., 1978, Composition and development of continental tectosphere: Nature, v. 274, p. 544-548.

Kay, R.W., and Kay, S.M., 1993, Delamination and delamination magmatism: Tectonophysics, v. 219, p. 177-189.

Kelemen, P.B., 1995, Genesis of high Mg-number andesites and the continental-crust: Contributions to Mineralogy and Petrology, v. 120, p. 1-19.

Kelemen, P.B., Shimizu, N., and Dunn, T., 1993, Relative depletion of niobium in some arc magmas and the continental-crust - partitioning of K, Nb, La and Ce during melt/rock reaction in the upper-mantle: Earth and Planetary Science Letters, v. 120, p. 111-134.

Keller, G.R., Braile, L.W., Mcmechan, G.A., Thomas, W.A., Harder, S.H., Chang, W.F., and Jardine, W.G., 1989, Paleozoic Continent-Ocean Transition in the Ouachita Mountains Imaged from Passcal Wide-Angle Seismic Reflection-Refraction Data: Geology, v. 17, p. 119-122.

Keller, G.R., and Hatcher, R.D., 1999, Some comparisons of the structure and evolution of the southern Appalachian-Ouachita orogen and portions of the Trans-European Suture Zone region: Tectonophysics, v. 314, p. 43-68.

King, P.B., 1975, The Ouachita and Appalachian orogenic belts, *in* Nairn, A.S., FG, ed., The ocean basins and margins: New York, NY, Plenum Press, p. 201-241.

Klemme, S., 2004, The influence of Cr on the garnet-spinel transition in the Earth's mantle: experiments in the system MgO-Cr2O3-SiO2 and thermodynamic modelling: Lithos, v. 77, p. 639-646.

Lambert, D.D., Shirey, S.B., and Bergman, S.C., 1995, Proterozoic lithospheric mantle source for the Prairie-Creek lamproites - Re-Os and Sm-Nd isotopic evidence: Geology, v. 23, p. 273-276.

Lee, C.T.A., 2005, Trace element evidence for hydrous metasomatism at the base of the North American lithosphere and possible association with Laramide low-angle subduction: Journal of Geology, v. 113, p. 673-685.

Lee, C.T.A., Harbert, A., and Leeman, W.P., 2007a, Extension of lattice strain theory to mineral/mineral rare-earth element partitioning: An approach for assessing disequilibrium and developing internally consistent partition coefficients between

olivine, orthopyroxene, clinopyroxene and basaltic melt: Geochimica Et Cosmochimica Acta, v. 71, p. 481-496.

Lee, C.T.A., Morton, D.M., Kistler, R.W., and Baird, A.K., 2007b, Petrology and tectonics of Phanerozoic continent formation: From island arcs to accretion and continental arc magmatism: Earth and Planetary Science Letters, v. 263, p. 370-387.

Longerich, H.P., Jackson, S.E., and Gunther, D., 1996, Laser ablation inductively coupled plasma mass spectrometric transient signal data acquisition and analyte concentration calculation: Journal of Analytical Atomic Spectrometry, v. 11, p. 899-904.

Lonsdale, J.T., 1927, The igneous rocks of the Balcones Fault region of Texas: Austin, University of Texas Bulletin p. 178.

McDonough, W.F., and Sun, S.s., 1995, The composition of the Earth: Chemical Geology, v. 120, p. 223-253.

Mickus, K.L., and Keller, G.R., 1992, Lithospheric structure of the south-central United-States: Geology, v. 20, p. 335-338.

Miggins, D.P.B., Charles D; Smith, David V, 2004, Preliminary (super 40) Ar/ (super 39) Ar geochronology of igneous intrusions from Uvalde County, Texas; defining a more precise eruption history for the southern Balcones volcanic province: Open-File Report - USGS, Report: OF 2004-1031, p. 31.

Miser, H.D., 1934, Relation of Ouachita belt of Paleozoic rocks to oil and gas fields of MidContinent region: Bulletin of the American Association of Petroleum Geologists, v. 18, p. 1059-1077.

Mosher, S., 1998, Tectonic evolution of the southern Laurentian Grenville orogenic belt: Geological Society of America Bulletin, v. 110, p. 1357-1375.

Mosher, S., Levine, J.S.F., and Carlson, W.D., 2008, Mesoproterozoic plate tectonics: A collisional model for the Grenville-aged orogenic belt in the Llano uplift, central Texas: Geology, v. 36, p. 55-58.

Nelson, B.K., and Depaolo, D.J., 1985, Rapid production of continental-crust 1.7 to 1.9b.Y. ago - Nd isotopic evidence from the basement of the North-American mid-continent: Geological Society of America Bulletin, v. 96, p. 746-754.

Niu, Y.L., 1997, Mantle melting and melt extraction processes beneath ocean ridges: Evidence from abyssal peridotites: Journal of Petrology, v. 38, p. 1047-1074.

Peslier, A.H., Francis, D., and Ludden, J., 2002, The lithospheric mantle beneath continental margins; melting and melt-rock reaction in Canadian Cordillera xenoliths: Journal of Petrology, v. 43, p. 2013-2047.

Pickering, K.T., 1989, The destruction of Iapetus and Tornquist's Oceans: Geology Today, v. 5, p. 160-166.

Pickering, K.T., and Smith, A.G., 1995, Arcs and backarc basins in the Early Paleozoic Iapetus Ocean: The Island Arc, v. 4, p. 1-67.

Pollack, H.N., Hurter, S.J., and Johnson, J.R., 1993, Heat-Flow from the Earth's Interior - Analysis of the Global Data Set: Reviews of Geophysics, v. 31, p. 267-280.

Rankin, D.W., 1994, Continental margin of the Eastern United States; past and present, *in* Speed, R.C., ed.: Boulder, Geological Society of America.

Ringwood, A.E., 1975, Composition and petrology of the Earth's mantle, McGraw-Hill, 617 p.

Rivers, T., Vangool, J.A.M., and Connelly, J.N., 1993, Contrasting tectonic styles in the northern Grenville Province - implications for the dynamics of orogenic fronts: Geology, v. 21, p. 1127-1130.

Rudnick, R.L., 1995, Making continental-crust: Nature, v. 378, p. 571-578.

Ryerson, F.J., and Watson, E.B., 1987, Rutile saturation in magmas - implications for Ti-Nb-Ta depletion in island-arc basalts: Earth and Planetary Science Letters, v. 86, p. 225-239.

Spencer, A.B., 1969, Alkalic igneous rocks of Balcones Province, Texas: Journal of Petrology, v. 10, p. 272-&.

Thomas, W.A., 1991, The Appalachian-Ouachita rifted margin of southeastern North-America: Geological Society of America Bulletin, v. 103, p. 415-431.

Thomas, W.A., and Astini, R.A., 1996, The Argentine precordillera: A traveler from the Ouachita Embayment of North American Laurentia: Science, v. 273, p. 752-757.

Torsvik, T.H., Smethurst, M.A., Meert, J.G., VanderVoo, R., McKerrow, W.S., Brasier, M.D., Sturt, B.A., and Walderhaug, H.J., 1996, Continental break-up and collision in the Neoproterozoic and Palaeozoic - A tale of Baltica and Laurentia: Earth-Science Reviews, v. 40, p. 229-258.

Turner, S.P., Kelley, S.P., VandenBerg, A.H.M., Foden, J.D., Sandiford, M., and Flottmann, T., 1996, Source of the Lachlan fold belt flysch linked to convective removal of the lithospheric mantle and rapid exhumation of the Delamerian-Ross fold belt: Geology, v. 24, p. 941-944.

Van Schmus, W.R., Bickford, M.E., Turek, A., 1996, Proterozoic geology of the east-central Midcontinent basement, *in* Van der Pluijm, B.A., ed., Basements and Basins of Eastern North America, Geological Society of America, p. 7-33.

Walker, N., 1992, Middle Proterozoic geologic evolution of Llano Uplift, Texas - evidence from U-Pb zircon geochronometry: Geological Society of America Bulletin, v. 104, p. 494-504.

Walter, M.J., Heinrich, D.H., and Karl, K.T., 2003, Melt extraction and compositional variability in mantle lithosphere, Treatise on Geochemistry: Oxford, Pergamon, p. 363-394.

Walter, M.J., Sisson, T.W., and Presnall, D.C., 1995, A mass proportion method for calculating melting reactions and application to melting of model upper mantle lherzolite: Earth and Planetary Science Letters, v. 135, p. 77-90.

Wegener, A., 2001, The origins of the continents: Journal of Geodynamics, v. 32, p. 29-63.

Wells, P.R.A., 1977, Pyroxene thermometry in simple and complex systems: Contributions to Mineralogy and Petrology, v. 62, p. 129-139.

Woodruff, C.M., and Foley, D., 1985, Thermal regimes of Balcones-Ouachita trend, central Texas: AAPG Bulletin-American Association of Petroleum Geologists, v. 69, p. 1431-1431.

Yaxley, G.M., Crawford, A.J., and Green, D.H., 1991, Evidence for carbonatite metasomatism in spinel peridotite xenoliths from western Victoria, Australia: Earth and Planetary Science Letters, v. 107, p. 305-317.

CAPTIONS:

Figure 1: ArcGIS generated map of the North American continent showing the location of Knippa samples, coastlines and state boundaries, and other features. The outline of the gravity anomaly in eastern North America is traced from GeoNet (PACES) gravity data of the conterminous United States. The location of Proterozoic outcrop is reproduced from the USGS Geologic Map of the United States and the Grenville Front reproduced generally from Hoffman (1988). Also shown is the trace A – A' of a regional cross-section by Mickus and Keller, 1992.

Figure 2: The raw data output of the ICP-MS for one cpx from sample 05A. The first 10 counts are the background intensities. The analyzed data signal chosen from this shot is shown in Fig. 2b. Notice that Cs (bold, no marker) is variably enriched, but we eliminated that part of the signal that was not parallel to the other elements.

Figure 3: Using models of Pollack and Chapman (1993), we calculate the P-T profile for continents under various surface heat flow conditions. The range of P-T conditions for the Knippa samples is constrained by their calculated temperatures of equilibration, the 85 km spinel-garnet transition, and reasonable geotherms (modern day surface heat flux of ~50 mW/m^2 is consistent with a cool, thick lithosphere).

Figure 4: (a-c) Variation of MgO with (a) CaO, (b) Na_2O, and (c) Al_2O_3 in Knippa samples and other types of peridotites. Abyssal peridotites are dominated by varying degrees of melt depletion. The loss of CaO and gain of MgO is indicative of previous loss of basaltic melt. (d) The direct correlation of moderately incompatible trace elements such as Lu with CaO is also consistent with depletion by partial melting of a fertile source.

Figure 5: (a) The bulk concentration of trace elements in each sample of this study, normalized to PM. Elements ordered to reflect thermodynamic similarity under anhydrous conditions. Most samples from the Knippa locality preferentially enriched in LREE's over Nb, Ta, and Pb as well as preferentially enriched in MREE's over Zr, Hf, and Ti. Samples 01A and 08A do not fit the general pattern, although these samples have the most refractory mineral modes. (b) Theoretically calculated, PM normalized concentration of elements in a depleted, unserpentinized mantle residue; Also shows concentrations of elements in an anhydrous 1% melt of fertile mantle. Samples from this study are in the blue field. The two curves which pass through the sample field are the result of mixing the depleted residue with the basaltic melt (high HFSE) or a HFSE depleted melt/fluid.

Figure 6: The bulk concentration of La/Sm versus Sm/Yb for the Knippa samples, PUM (McDonough and Sun, 1995), continental arc material, Cascadian xenoliths, SE Australian carbonatite-influenced xenoliths (Yaxley et al., 1991), and global oceanic peridotites (Niu et al., 1997). The Knippa and continental materials all have La/Sm ratios above PM, while oceanic materials have La/Sm and Sm/Yb ratios lower than PM. Only the Yaxley samples have significant MREE enrichment.

Figure 7: Mulitelement, PM-normalized spidergram for several cpx grains from the same xenolith (05A). Notice the variability in concentration of Cs, Rb, Ba between different textures and between grains of turbid texture. For this reason, bulk abundances of these elements are very uncertain.

Figure 8: The ratio of the concentration of REE's in orthpyroxene over clinopyroxene versus decreasing cationic lattice radius in the cores of minerals from sample 05A of this study. The trend is typical of all samples in the study, including the negative divergence from theory at Eu. The data is plotted with the theoretical partition coefficients calculated from lattice strain theory by Lee et al. (2007). When equilibrium is achieved, the partition coefficients (Dopx/cpx) ~ K (the equilibrium constant) ~ (Copx/cpx). The plot shows that the samples analyzed are in fact in thermodynamic equilibrium for the REE's.

FIGURE 1

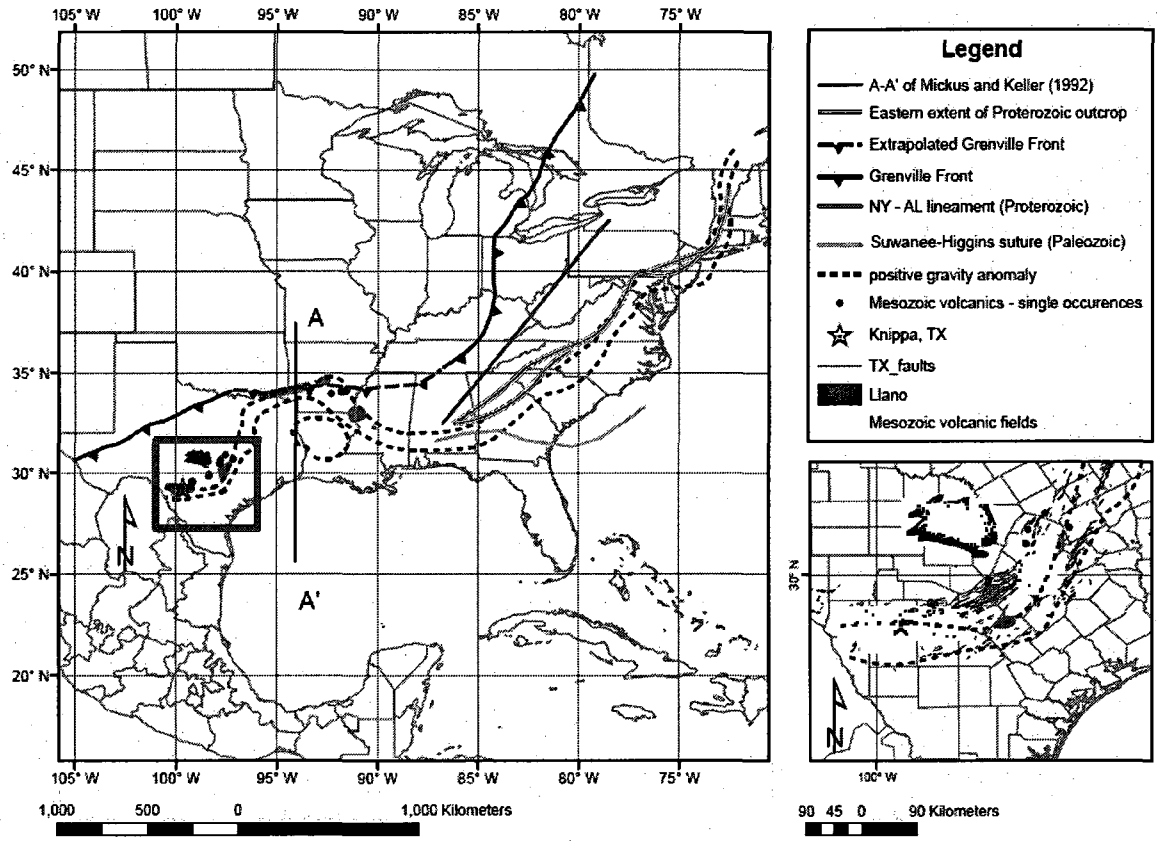
105° W
100° W
95° W
90° W
85° W
80° W
75° W
50° N
45° N
40° N
35° N
30° N
25° N
20° N
A
A'
N
1,000 500 0 1,000 Kilometers
Legend
A-A' of Mickus and Keller (1992)
Eastern extent of Proterozoic outcrop
Extrapolated Grenville Front
Grenville Front
NY - AL lineament (Proterozoic)
Suwanee-Higgins suture (Paleozoic)
positive gravity anomaly
Mesozoic volcanics - single occurences
Knippa, TX
TX_faults
Llano
Mesozoic volcanic fields
30° N
100° W
90 45 0 90 Kilometers

FIGURE 2

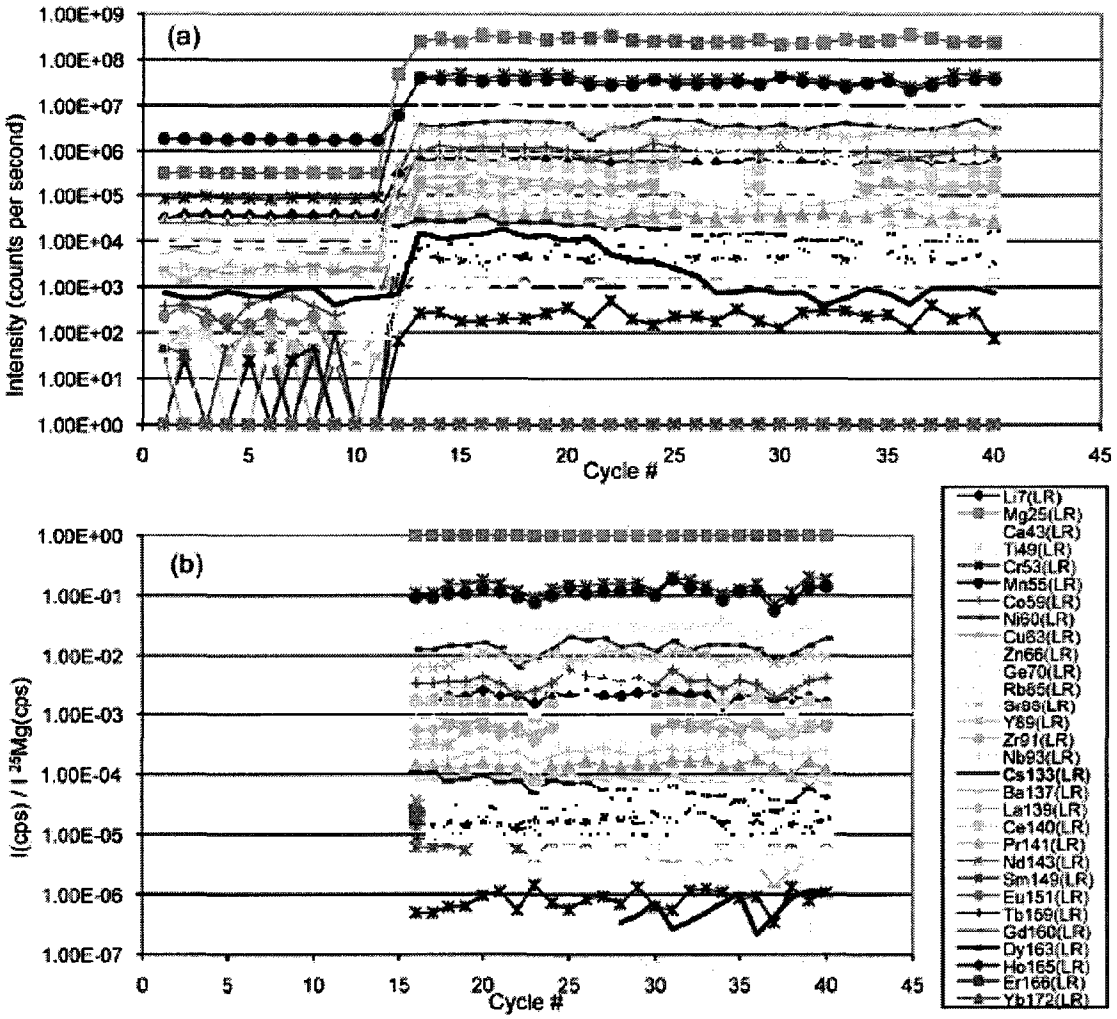
(a)
Intensity (counts per second)
1.00E+09
1.00E+08
1.00E+07
1.00E+06
1.00E+05
1.00E+04
1.00E+03
1.00E+02
1.00E+01
1.00E+00
0
5
10
15
20
25
30
35
40
45
Cycle #
(b)
I(cps) / I 25Mg(cps)
1.00E+00
1.00E-01
1.00E-02
1.00E-03
1.00E-04
1.00E-05
1.00E-06
1.00E-07
Cycle #
Li7(LR)
Mg25(LR)
Ca43(LR)
Ti49(LR)
Cr53(LR)
Mn55(LR)
Co59(LR)
Ni60(LR)
Cu63(LR)
Zn66(LR)
Ge70(LR)
Rb85(LR)
Sr88(LR)
Y89(LR)
Zr91(LR)
Nb93(LR)
Cs133(LR)
Ba137(LR)
La139(LR)
Ce140(LR)
Pr141(LR)
Nd143(LR)
Sm149(LR)
Eu151(LR)
Tb159(LR)
Gd160(LR)
Dy163(LR)
Ho165(LR)
Er166(LR)
Yb172(LR)

FIGURE 3

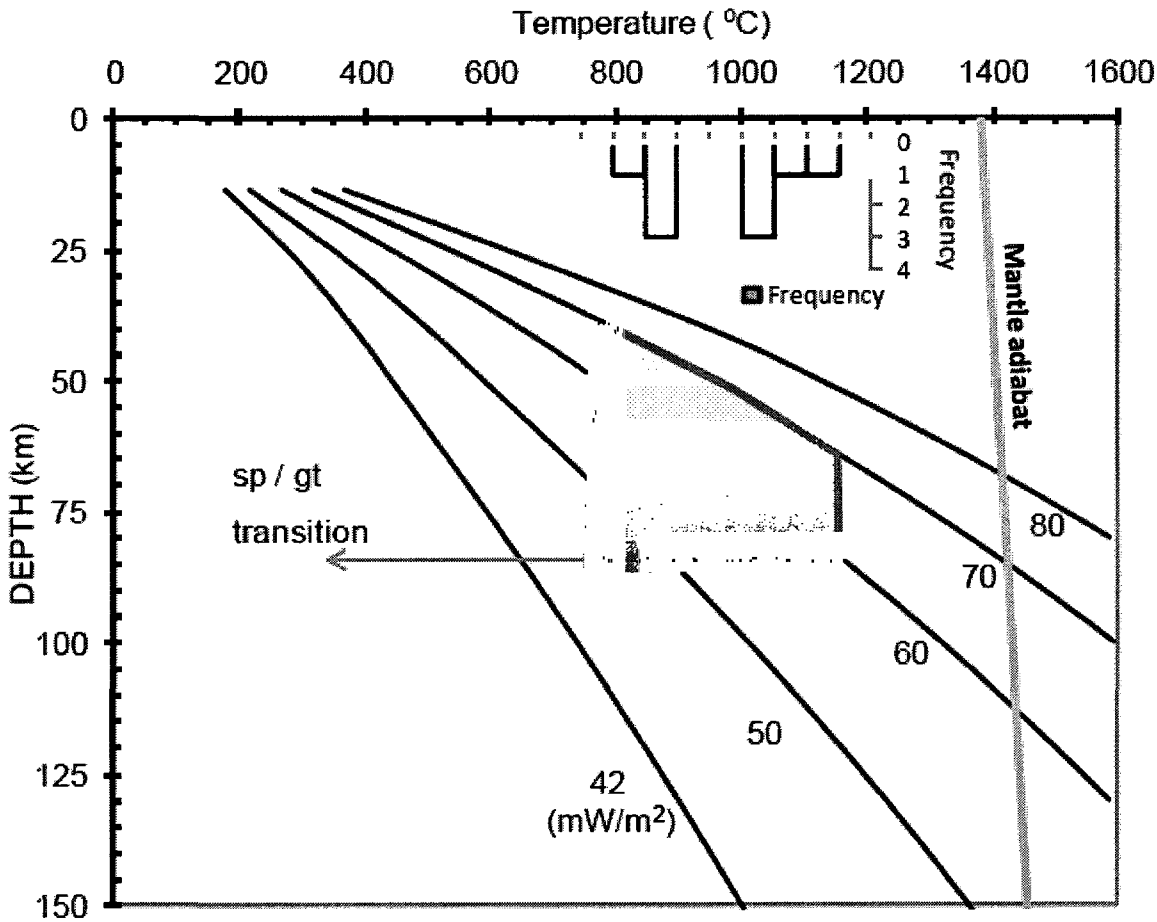
Temperature (°C)
0
200
400
600
800
1000
1200
1400
1600
DEPTH (km)
0
25
50
75
100
125
150
0
1
2
3
4
Frequency
Frequency
Mantle adiabat
sp / gt
transition
80
70
60
50
42
(mW/m2)

FIGURE 4

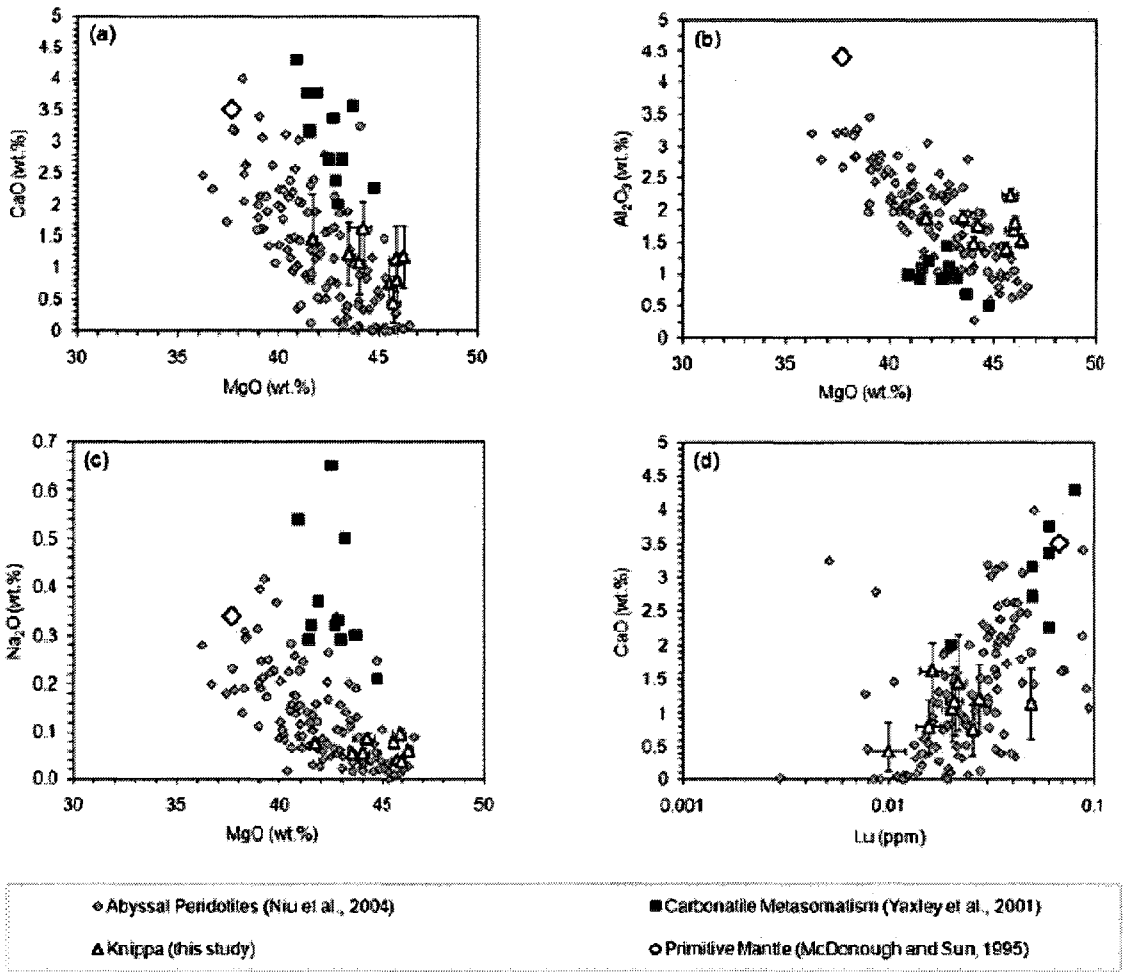
(a)
CaO (wt.%)
MgO (wt.%)
(b)
Al2O3 (wt.%)
MgO (wt.%)
(c)
Na2O (wt.%)
MgO (wt.%)
(d)
CaO (wt.%)
Lu (ppm)
Abyssal Peridotites (Niu et al., 2004)
Carbonatite Metasomatism (Yaxley et al., 2001)
Knippa (this study)
Primitive Mantle (McDonough and Sun, 1995)

FIGURE 5

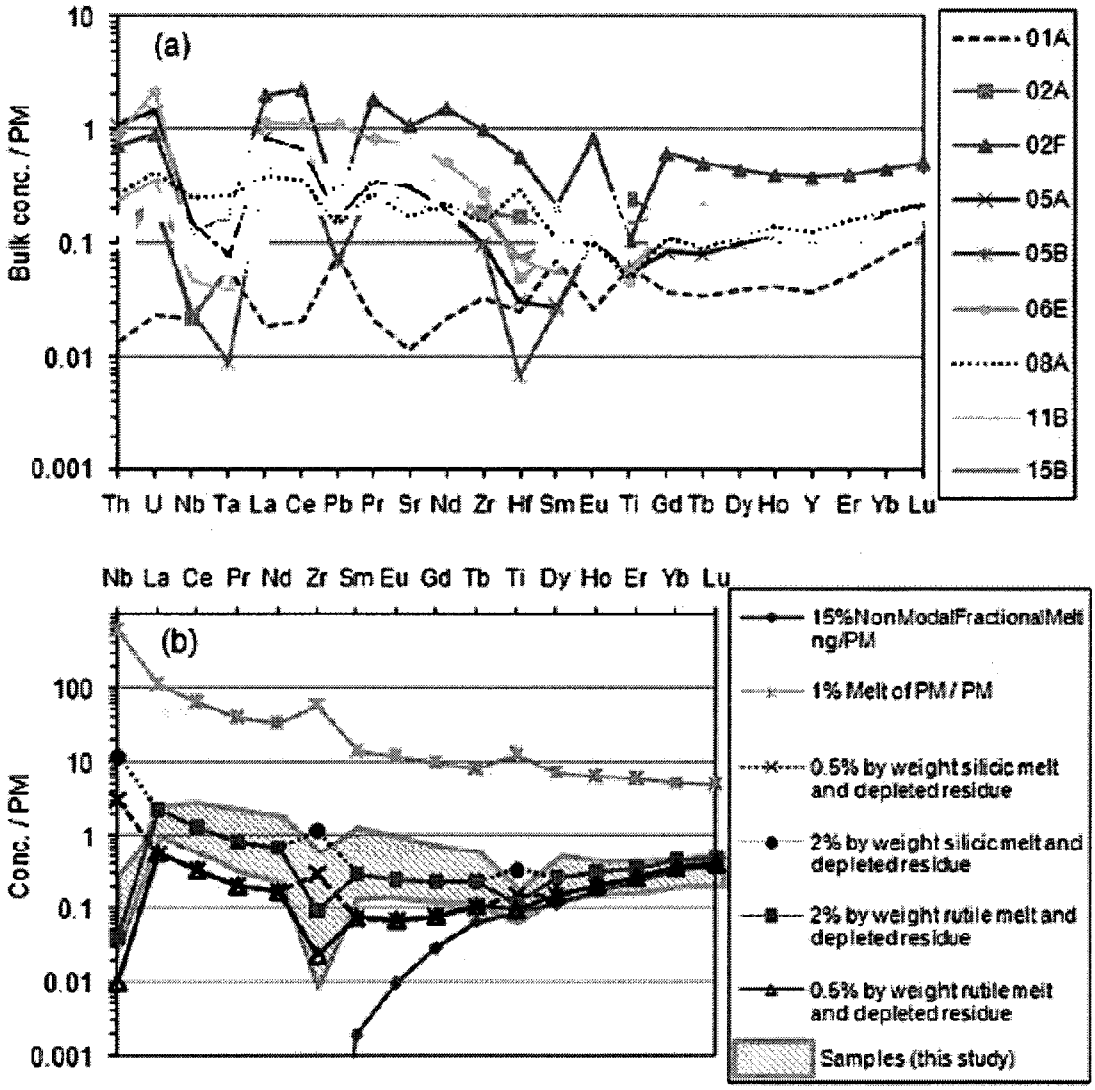
(a)
Bulk conc. / PM
10
1
0.1
0.01
0.001
Th U Nb Ta La Ce Pb Pr Sr Nd Zr Hf Sm Eu Ti Gd Tb Dy Ho Y Er Yb Lu
01A
02A
02F
05A
05B
06E
08A
11B
15B
Nb La Ce Pr Nd Zr Sm Eu Gd Tb Ti Dy Ho Er Yb Lu
(b)
Conc. / PM
100
10
1
0.1
0.01
0.001
15%NonModalFractionalMelting/PM
1% Melt of PM / PM
0.5% by weight silicic melt and depleted residue
2% by weight silicic melt and depleted residue
2% by weight rutile melt and depleted residue
0.5% by weight rutile melt and depleted residue
Samples (this study)

FIGURE 6

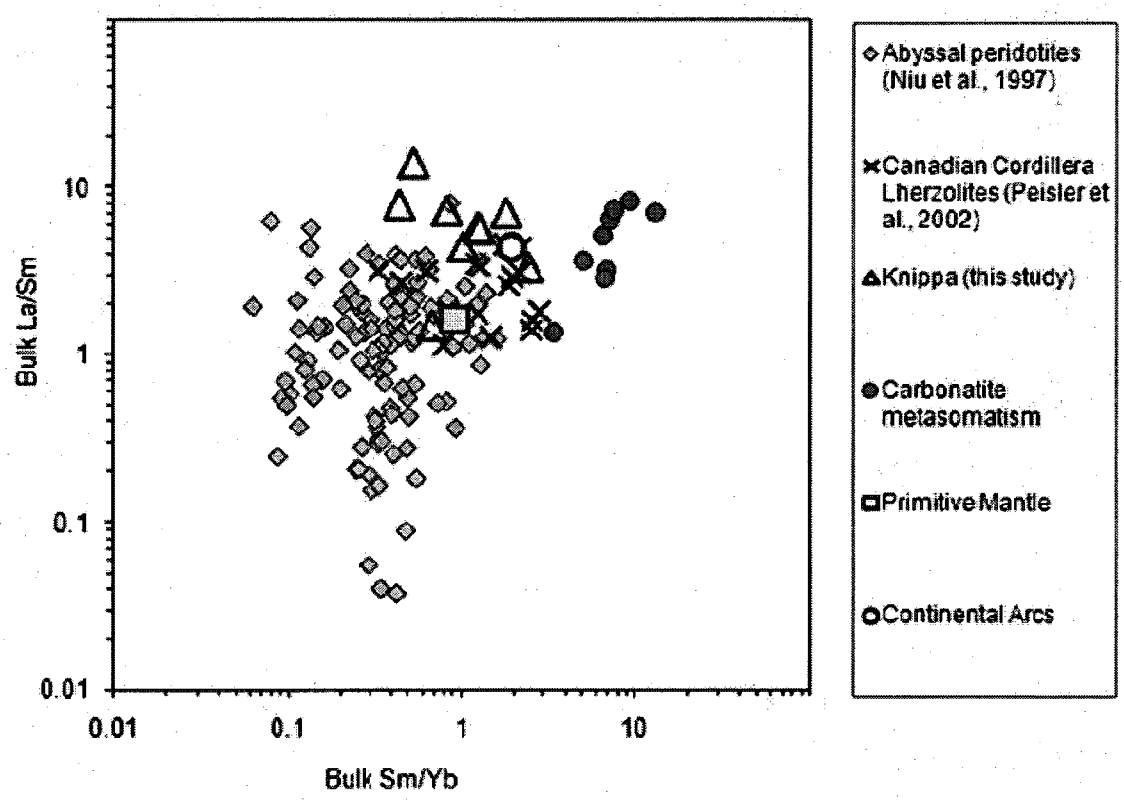
Bulk La/Sm
Bulk Sm/Yb
0.01
0.1
1
10
Abyssal peridotites (Niu et al., 1997)
Canadian Cordillera Lherzolites (Peisler et al., 2002)
Knippa (this study)
Carbonatite metasomatism
Primitive Mantle
Continental Arcs

FIGURE 7

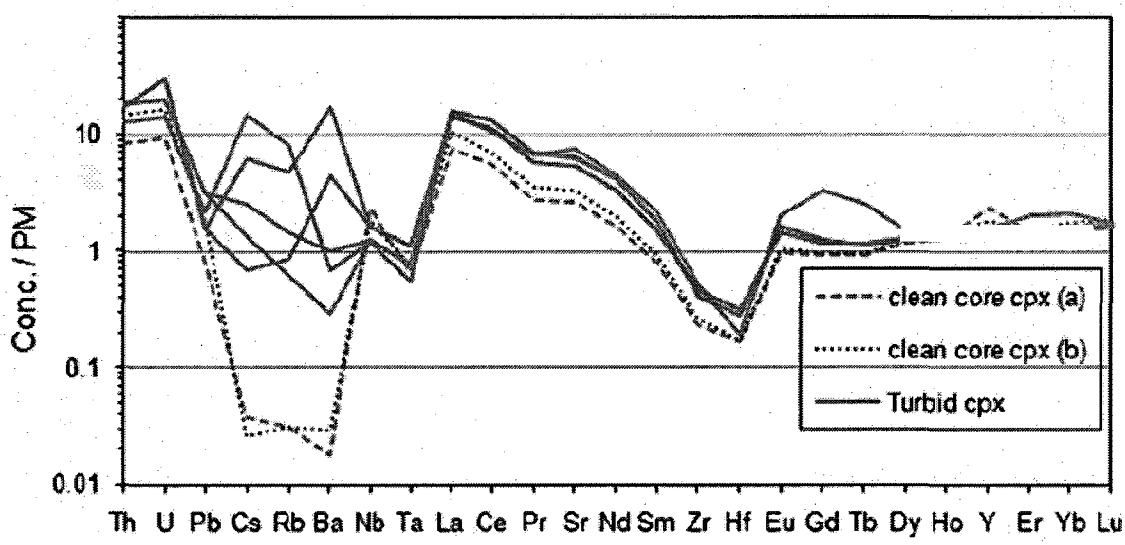
Conc. / PM
10
1
0.1
0.01
Th U Pb Cs Rb Ba Nb Ta La Ce Pr Sr Nd Sm Zr Hf Eu Gd Tb Dy Ho Y Er Yb Lu
clean core cpx (a)
clean core cpx (b)
Turbid cpx

FIGURE 8

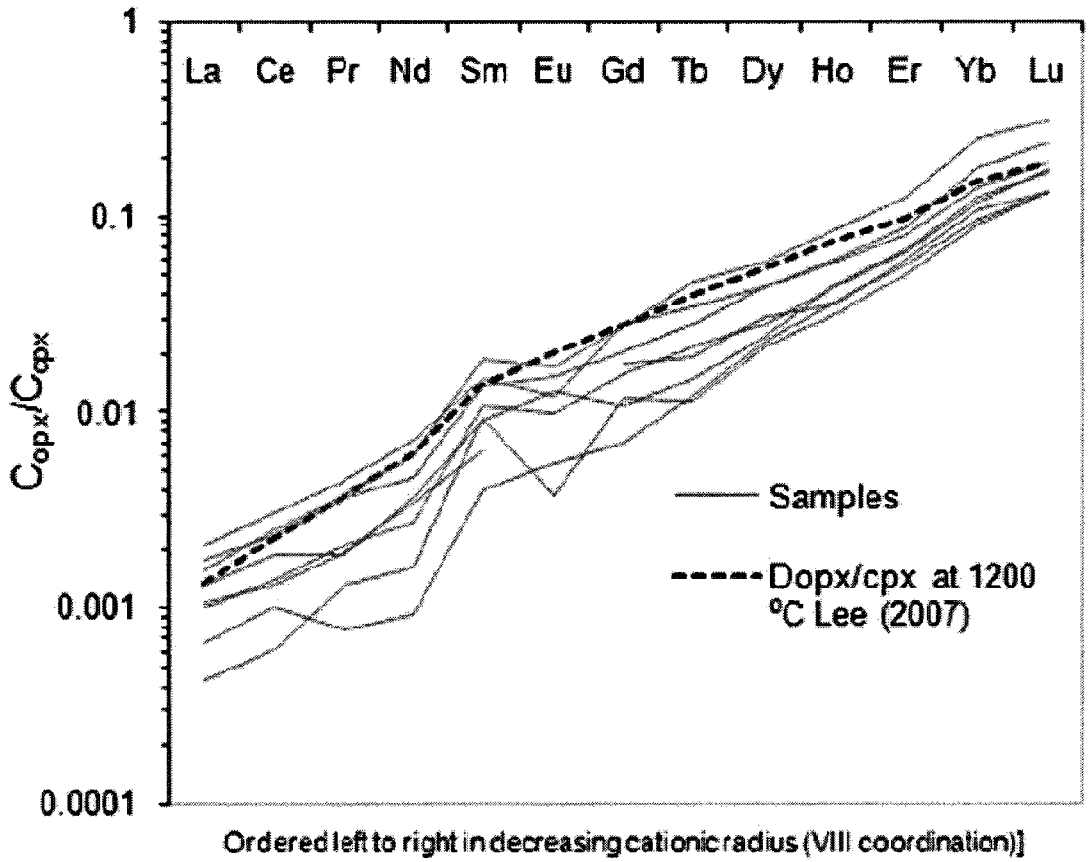
1
0.1
0.01
0.001
0.0001
La Ce Pr Nd Sm Eu Gd Tb Dy Ho Er Yb Lu
C_{opx}/C_{cpx}
Samples
Dopx/cpx at 1200 °C Lee (2007)
Ordered left to right in decreasing cationic radius (VIII coordination)]

TABLE 1. MINERAL MODES AND COMPOSITIONS

Sample	01A				02A				02F				05A				05B			
	ol	opx	cpx	sp	ol	opx	cpx	sp	ol	opx	cpx	sp (N/A)	ol	opx	cpx	sp	ol	opx	cpx	sp
Modes:	0.72	0.25	0.01	0.02	0.72	0.23	0.03	0.02	0.71	0.225	0.045	0.02	0.7	0.21	0.07	0.02	0.7	0.225	0.065	0.02
wt. %																				
SiO2	37.9	57.2	50.2	0.141	38.1	56.1	49.4	0.0497	40.3	57.2	52.2	N/A	40.0	60.1	56.0	0.162	42.4	62.5	57.1	0.126
TiO2	0.00796	0.0636	0.314	0.117	0.00465	0.117	0.487	0.440	0.00190	0.0397	0.179	N/A	0.000900	0.0281	0.132	0.0583	0.000893	0.0300	0.147	0.0508
Al2O3	0.818	2.60	3.14	48.1	0.0235	2.22	3.80	37.2	0.0347	3.30	3.87	N/A	0.0109	2.74	3.20	47.7	0.0115	3.03	2.85	50.1
Cr2O3	0.107	0.376	0.798	20.0	0.0105	0.363	1.14	24.6	0.0109	0.370	0.754	N/A	0.00973	0.382	0.808	17.5	0.00632	0.269	0.606	12.8
FeO	9.29	6.01	2.41	13.2	9.22	6.90	3.28	16.7	9.49	6.36	2.88	N/A	9.53	5.83	2.23	11.3	10.6	6.19	2.41	12.3
MnO	0.160	0.153	0.0867	0.146	0.130	0.167	0.0879	0.153	0.134	0.149	0.102	N/A	0.161	0.154	0.0868	0.137	0.192	0.173	0.0887	0.131
MgO	51.5	32.7	18.3	19.1	51.5	33.2	18.3	18.0	52.0	34.7	18.9	N/A	51.3	31.7	16.7	22.8	48.0	29.0	16.7	24.2
CaO	0.128	0.435	23.4	0.00	0.0378	0.393	21.5	0.00993	0.0562	0.562	21.7	N/A	0.0418	0.487	21.5	0.00460	0.0313	0.397	20.7	0.0118
Na2O	0.0319	0.0399	0.896	0.00	0.0324	0.0551	1.44	0.00780	0.00657	0.0929	1.57	N/A	0.00161	0.0637	1.02	0.00	0.00551	0.0700	0.895	0.00
K2O	0.00962	0.0123	0.00296	0.00	0.00873	0.0000469	0.0271	0.0181	0.00	0.00	0.0129	N/A	0.00	0.00107	0.00369	0.0106	0.00	0.00731	0.0607	0.00694
SUM	99.9	99.6	99.5	101	99.0	99.8	99.4	97.2	102	99.8	102	N/A	101	99.8	102	99.8	101	99.8	102	99.7
Mg#	90.6				90.4				90.5				90.5				89.0			

Trace conc.	01A				02A				02F				05A				05B			
ppm	ol	opx	cpx	sp	ol	opx	cpx	sp	ol	opx	cpx	sp (N/A)	ol	opx	cpx	sp	ol	opx	cpx	sp
Li	1.62	1.75	26.3	0.189	2.02	2.06	34.7	6.25	3.20	57.6	25.9	N/A	2.37	3.02	19.0	0.436	1.48	2.75	8.71	0.412
Ti	7.28	219	695	447	20.6	788	3190	59.1	5.23	304	1210	N/A	4.81	140	406	315	4.22	141	524	290
Cr	57.6	3140	5980	112000	49.7	2670	8320	4210	50.5	4050	11800	N/A	72.9	3020	6480	121000	52.3	2350	5070	98400
Mn	1070	1030	593	788	1090	1220	580	436	789	1970	1210	N/A	1220	1100	614	913	1390	1110	609	1010
Co	155	58.3	22.4	185	138	67.4	20.3	70.3	112	110	40.2	N/A	173	62.4	20.4	273	178	57.5	17.8	272
Ni	3360	780	348	1730	3220	809	284	1270	2410	1340	597	N/A	3190	846	298	2650	3520	708	206	3220
Cu	0.985	0.259	3.19	N/A	N/A	0.00647	2.47	0.306	N/A	N/A	N/A	N/A	1.17	0.919	3.54	5.29	0.157	0.265	0.518	2.25
Zn	57.8	37.7	11.2	N/A	N/A	39.9	12.8	59.4	N/A	N/A	N/A	N/A	54.1	34.4	10.1	914	70.2	38.7	12.1	1430
Y	0.00969	0.387	6.03	0.0102	0.0167	0.763	16.3	0.00925	0.0236	1.12	30.2	N/A	0.0120	0.335	5.51	0.00746	0.0135	0.395	8.34	0.0104
Cs	0.000965	0.000999	0.00322	0.0206	0.00191	0.00185	0.00730	0.0142	0.000155	BDL	0.606	N/A	0.000260	0.00116	0.0109	0.00162	0.0000867	0.00664	0.241	0.0122
Rb	0.00523	0.0466	0.155	0.486	0.100	0.0220	0.351	0.355	0.0154	0.141	6.89	N/A	0.00263	0.0149	0.234	0.0655	BDL	0.107	4.85	0.148
Ba	0.0722	0.0137	0.227	0.138	0.305	BDL	1.54	0.647	0.0462	0.372	24.0	N/A	0.0525	0.0674	8.03	0.0492	BDL	0.274	11.0	0.369
Nb	0.00240	0.0395	0.267	N/A	BDL	0.0325	0.225	N/A	0.00123	0.0822	1.31	N/A	0.00653	0.0713	1.16	N/A	BDL	0.0326	0.130	N/A
Ta	0.00220	0.00154	0.0244	0.0000512	0.00241	0.000402	0.0157	0.000409	BDL	0.00467	0.120	N/A	0.000736	0.00112	0.0309	0.00209	BDL	BDL	0.00506	0.000101
La	0.000238	0.00199	1.15	0.00294	0.00192	0.0150	14.4	0.00267	0.00155	0.0192	28.8	N/A	0.00146	0.0161	7.75	0.000890	BDL	0.00446	4.44	0.00457
Ce	0.00283	0.00728	3.13	0.00968	0.00743	0.0372	28.9	0.00607	0.00382	0.0853	83.7	N/A	0.00165	0.0467	15.5	0.00546	0.00101	0.0171	12.5	0.0129
Pr	0.000941	0.00156	0.431	0.00183	0.000720	0.00519	2.79	0.000562	0.000398	0.00801	10.4	N/A	0.000787	0.00526	1.20	BDL	BDL	0.00240	1.14	8DL
Sr	0.00852	0.0325	21.4	0.128	0.0193	0.292	363	0.962	0.0445	0.227	478	N/A	0.0207	0.159	88.1	0.0473	BDL	0.154	70.5	0.281
Nd	0.00244	0.0102	2.25	0.00229	BDL	0.0352	10.6	0.00443	0.00243	0.0395	42.8	N/A	0.00485	0.0247	3.44	0.00546	0.00400	0.00940	3.48	0.00811
Sm	0.00374	0.0110	0.806	0.00945	BDL	0.0149	2.39	0.000262	BDL	0.0344	8.81	N/A	0.00339	0.00761	0.516	0.00353	BDL	0.00605	0.558	BDL
Zr	0.0271	0.610	9.79	N/A	0.112	1.34	47.4	N/A	0.0708	0.653	130	N/A	0.00835	0.319	3.58	N/A	BDL	0.140	0.630	N/A
Hf	0.0119	0.0291	0.469	0.00280	0.00849	0.0114	0.944	0.00146	BDL	0.00897	1.27	N/A	0.00212	0.00785	0.0667	BDL	0.00440	0.00333	0.0535	BDL
Eu	0.000153	0.00425	0.282	BDL	0.000148	BDL	0.851	BDL	BDL	0.0152	2.78	N/A	0.00277	0.00238	0.195	0.00458	0.0000143	0.00247	0.251	0.00947
Gd	0.00510	0.0223	1.10	0.00392	0.00426	0.0483	2.76	BDL	BDL	0.0495	7.17	N/A	0.00184	0.0162	0.583	0.00245	0.00220	0.0126	0.805	0.00318
Tb	0.000763	0.00482	0.172	0.000537	BDL	0.00816	0.427	BDL	0.000869	0.0122	1.02	N/A	BDL	0.00354	0.104	BDL	0.000748	0.00345	0.158	0.000753
Dy	0.00222	0.0503	1.15	0.00481	0.00503	0.0881	2.94	BDL	0.00333	0.134	5.91	N/A	0.00192	0.0361	0.833	0.000918	0.00137	0.0377	1.33	0.00579
Ho	0.000752	0.0138	0.232	BDL	0.00130	0.0207	0.592	0.000370	0.000783	0.0396	1.09	N/A	0.000676	0.0120	0.202	0.000231	0.000659	0.0140	0.316	0.000350
Er	0.00385	0.0536	0.613	BDL	BDL	0.0975	1.62	BDL	0.00552	0.167	2.96	N/A	0.00265	0.0515	0.641	BDL	0.00260	0.0623	0.953	BDL
Yb	0.00765	0.0936	0.520	0.00370	0.0131	0.153	1.44	0.00337	0.0128	0.266	2.82	N/A	0.00916	0.101	0.711	BDL	BDL	0.116	0.985	0.00363
Lu	0.00345	0.0185	0.0773	0.000577	0.00297	0.0280	0.214	0.00155	0.00364	0.0561	0.427	N/A	0.00290	0.0220	0.117	BDL	0.00330	0.0284	0.164	BDL
Pb	0.00200	0.00602	0.0645	0.421	0.0228	0.00365	1.19	0.0295	0.00772	0.0294	0.497	N/A	0.00749	0.00582	0.275	0.00578	0.00479	0.00492	0.0886	0.0107
Th	0.000638	0.000758	0.0447	BDL	BDL	0.00296	0.334	BDL	0.00139	0.0112	1.20	N/A	0.00222	0.0113	1.17	0.00151	0.000508	0.00168	0.170	0.000596
U	BDL	0.000724	0.0267	0.00145	0.00163	0.00189	0.0956	0.000352	0.000573	0.0133	0.331	N/A	0.000698	0.00855	0.384	0.000603	0.000165	0.000932	0.0655	0.00125

TABLE 1. (continued)

Sample	06E				08A				11B				15B			
	ol	opx	cpx	sp (N/A)	ol	opx	cpx	sp	ol	opx	cpx	sp	ol	opx	cpx	sp
Modes:	0.7	0.235	0.045	0.02	0.71	0.24	0.03	0.02	0.71	0.22	0.05	0.02	0.7	0.23	0.05	0.02
wt. %																
SiO2	40.0	58.7	56.4	N/A	40.2	58.4	51.0	0.105	38.3	53.8	50.5	0.290	40.9	56.0	50.6	0.656
TiO2	0.00182	0.0367	0.266	N/A	0.00114	0.0329	0.214	0.0551	0.000800	0.0296	0.131	0.103	0.00164	0.0573	0.257	0.0942
Al2O3	0.0244	2.48	2.92	N/A	0.00705	3.16	3.19	46.8	0.00400	2.74	2.65	39.0	0.0116	3.40	3.21	46.9
Cr2O3	0.0103	0.359	0.703	N/A	0.00919	0.372	1.08	17.2	0.00856	0.565	0.928	23.2	0.0100	0.388	0.716	18.5
FeO	10.4	5.89	2.60	N/A	10.6	6.38	2.60	11.8	10.4	7.72	2.38	13.5	9.47	5.89	2.40	11.7
MnO	0.164	0.141	0.0447	N/A	0.173	0.151	0.0970	0.120	0.139	0.169	0.0715	0.126	0.136	0.140	0.0843	0.112
MgO	50.5	32.0	18.1	N/A	52.2	33.0	20.4	21.1	52.4	35.5	17.8	21.0	49.3	33.1	19.7	19.8
CaO	0.0426	0.369	21.3	N/A	0.0397	0.484	22.0	0.00869	0.0265	0.419	21.3	0.0190	0.0332	0.464	21.7	0.00
Na2O	0.00418	0.0394	0.982	N/A	0.00130	0.0659	0.629	0.00555	0.00322	0.0500	0.970	0.00	0.00527	0.0545	0.745	0.00474
K2O	0.00	0.0220	0.180	N/A	0.00	0.00	0.0622	0.0101	0.00	0.0122	0.0310	0.00500	0.00	0.000165	0.0160	0.000195
SUM	101	99.8	104	N/A	103	99.8	101	97.3	101	99.8	96.7	97.3	99.9	99.8	99.5	97.8
Mg#	89.6				89.8				90.3				90.3			

Trace conc.	06E				08A				11B				15B			
	ol	opx	cpx	sp (N/A)	ol	opx	cpx	sp	ol	opx	cpx	sp	ol	opx	cpx	sp
Li	4.44	1.51	2.81	N/A	3.38	2.37	25.6	2.18	2.21	2.12	28.2	0.769	5.47	4.30	1.46	0.00
Ti	7.68	0.0133	1070	N/A	5.08	130	526	347	4.84	160	345	703	8.04	302	1930	510
Cr	67.2	0.0378	6940	N/A	68.9	3330	6570	112000	66.9	3380	5830	157000	44.8	2520	7890	123000
Mn	1180	0.392	598	N/A	1290	1130	662	805	1110	1160	490	989	943	955	785	724
Co	176	0.526	24.3	N/A	188	57.5	29.3	227	158	65.7	19.8	250	121	49.8	38.3	191
Ni	3290	0.583	360	N/A	3990	901	425	2120	3200	834	286	1550	2970	665	682	2050
Cu	0.929	0.0165	1.23	N/A	BDL	BDL	BDL	5.58	0.518	0.328	3.10	3.60	N/A	N/A	N/A	N/A
Zn	58.0	0.379	11.0	N/A	BDL	BDL	BDL	789	56.7	38.0	9.15	976	N/A	N/A	N/A	N/A
Y	0.0201	0.0237	10.4	N/A	0.0255	0.600	12.5	0.0199	0.0127	0.522	6.69	0.0216	0.0121	0.402	12.0	0.00188
Cs	BDL	2.94	0.103	N/A	0.000542	0.000747	0.00733	0.0504	BDL	0.00183	0.000393	BDL	0.00203	0.00	0.109	0.00165
Rb	BDL	2.63	2.87	N/A	0.0277	0.0689	0.0999	1.23	BDL	0.0135	0.0443	0.0700	0.0400	0.0128	1.72	0.0226
Ba	BDL	0.0679	20.1	N/A	0.112	0.202	1.26	2.12	0.0111	0.00	0.223	0.237	0.0155	0.000405	0.854	BDL
Nb	0.00461	0.0537	0.913	N/A	0.0156	0.338	2.35	N/A	0.00466	0.0556	0.310	N/A	0.00241	0.0104	0.875	N/A
Ta	0.000859	0.0105	0.0319	N/A	0.0000107	0.00177	0.295	0.00610	BDL	0.00153	0.0207	0.00293	0.00196	0.00	0.0482	0.00256
La	0.000645	0.168	15.8	N/A	BDL	0.0107	8.34	0.00988	BDL	0.0124	7.96	0.00676	0.000550	0.00413	9.68	BDL
Ce	0.00373	0.246	39.8	N/A	0.0111	0.0351	19.4	0.0194	0.00293	0.0505	20.3	0.0226	0.00178	0.00852	13.9	0.00296
Pr	0.00185	0.133	3.95	N/A	0.00196	0.00401	2.20	0.00155	0.000883	0.00777	2.11	0.00222	0.00	0.00143	1.11	0.00113
Sr	0.00177	0.206	327	N/A	0.00908	0.104	109	1.23	0.00260	0.234	149	0.595	0.0301	0.105	205	0.0417
Nd	BDL	0.0867	13.5	N/A	0.00212	0.0320	8.81	0.00269	BDL	0.0452	7.58	0.0151	0.00	0.00646	4.04	0.00451
Sm	BDL	0.0386	2.29	N/A	0.00470	0.0160	1.82	0.00436	0.00364	0.0242	1.30	0.00991	0.0144	0.0114	1.23	0.0129
Zr	0.0174	0.0144	10.9	N/A	0.160	3.58	69.3	N/A	0.0131	0.828	11.1	N/A	0.0120	0.291	14.2	N/A
Hf	0.00417	0.0304	0.331	N/A	0.00575	0.0296	0.608	0.00594	BDL	0.0172	0.231	0.00235	0.00147	0.0176	0.515	BDL
Eu	BDL	BDL	0.824	N/A	0.00129	0.00538	0.426	0.000474	0.00284	0.00710	0.422	BDL	0.000406	0.00202	0.546	0.00175
Gd	0.00100	0.0253	1.98	N/A	BDL	0.0190	1.81	BDL	0.00701	0.0360	1.33	BDL	0.00230	0.0210	1.82	BDL
Tb	BDL	0.0316	0.293	N/A	0.000442	0.00376	0.260	0.000778	BDL	0.00918	0.198	BDL	0.000289	0.00360	0.321	BDL
Dy	0.00261	0.0231	1.84	N/A	0.00349	0.0475	1.96	0.00293	BDL	0.0724	1.25	BDL	0.00196	0.0447	2.10	0.00481
Ho	BDL	0.0222	0.394	N/A	0.00160	0.0217	0.484	0.000399	BDL	0.0222	0.259	BDL	0.000740	0.0150	0.472	0.000909
Er	0.00761	0.0195	1.10	N/A	0.00626	0.0902	1.36	0.00154	0.00407	0.0847	0.693	BDL	0.00356	0.0640	1.29	BDL
Yb	0.0169	0.0282	1.11	N/A	0.0133	0.148	1.19	BDL	0.0127	0.150	0.609	BDL	0.0100	0.113	1.25	BDL
Lu	0.00616	0.0514	0.175	N/A	0.00363	0.0304	0.182	0.000709	0.00312	0.0279	0.0911	0.000266	0.00334	0.0221	0.169	0.00343
Pb	0.00247	0.625	0.392	N/A	0.00685	0.0186	0.412	0.0106	0.0133	0.00570	0.795	0.0375	0.00541	0.00331	0.461	0.00644
Th	BDL	0.0750	1.20	N/A	0.00151	0.00426	0.628	0.00997	0.00236	0.00496	0.326	0.00191	0.000533	BDL	0.139	0.000494
U	0.000100	0.126	0.320	N/A	0.000546	0.00401	0.232	0.00600	0.00144	0.00489	0.0999	0.00210	0.000293	0.00102	0.0843	BDL

TABLE 2. BULK COMPOSITION

	01A	02A	02F	05A	05B	06E	08A	11B	15B
Modes									
Ol	0.72	0.72	0.71	0.7	0.7	0.7	0.71	0.71	0.7
opx	0.25	0.23	0.225	0.21	0.225	0.235	0.24	0.22	0.23
cpx	0.01	0.03	0.045	0.07	0.065	0.045	0.03	0.05	0.05
sp	0.02	0.02	0.02	0.02	0.02	0.02	0.02	0.02	0.02
wt. %									
SiO2	42.1	41.8	43.8	44.6	47.4	44.3	44.1	41.6	44.1
TiO2	0.0271	0.0536	0.0271	0.0170	0.0179	0.0307	0.0162	0.0157	0.0291
Al2O3	2.23	1.39	1.69	1.76	1.88	1.48	1.80	1.52	1.89
Cr2O3	0.579	0.618	0.617	0.494	0.360	0.615	0.473	0.641	0.501
FeO	8.48	8.66	8.64	8.28	9.20	9.15	9.36	9.48	8.34
MnO	0.158	0.138	0.137	0.154	0.181	0.153	0.164	0.142	0.134
MgO	45.8	45.6	45.9	44.2	41.7	44.0	46.0	46.3	43.5
CaO	0.434	0.762	1.14	1.63	1.46	1.07	0.805	1.18	1.22
Na2O	0.0419	0.0793	0.0966	0.0862	0.0778	0.0565	0.0357	0.0618	0.0536
K2O	0.0100	0.00747	0.000942	0.000696	0.00607	0.0144	0.00357	0.00433	0.00355
SUM	99.8	99.1	102	101	102	101	103	101	99.7
Mg# in ol.	90.6	90.4	90.5	90.5	89.0	89.6	89.8	90.3	90.3
Eq. temp. °C (Wells 1977)	873	891	893	1034	1142	1066	1040	864	1007
TBKN (1.5-2.0 gigapascal)	782 to 789	862 to 870	848 to 856	1019 to 1028	1088 to 1078	1066 to 1078	977 to 986	820 to 827	955 to 963

Trace conc. (ppm)	01A	02A	02F	05A	05B	06E	08A	11B	15B
Li	1.87	3.10	16.4	3.63	2.23	3.59	3.78	3.46	4.89
Ti	76.0	293	126	67.4	74.6	53.6	57.6	70.0	182
Cr	3130	983	1480	3570	2860	360	3290	4220	3470
Mn	1050	1090	1060	1140	1280	852	1220	1080	934
Co	130	117	106	141	144	124	153	133	102
Ni	2650	2540	2040	2490	2700	2320	3110	2500	2300
Cu	0.806	0.0816	N/A	1.37	0.248	0.710	N/A	N/A	N/A
Zn	51.1	10.8	N/A	64.1	87.1	41.2	N/A	N/A	N/A
Y	0.164	0.677	1.63	0.465	0.641	0.489	0.539	0.459	0.702
Cs	0.00139	0.00231	0.0274	0.00122	0.0175	0.696	0.00179	0.000422	0.00691
Rb	0.0267	0.0949	0.353	0.0227	0.342	0.748	0.0639	0.00659	0.117
Ba	0.0605	0.279	1.20	0.614	0.782	0.922	0.208	0.0238	0.0536
Nb	0.0143	0.0142	0.0781	0.101	0.0158	0.0569	0.163	0.0311	0.0478
Ta	0.00221	0.00231	0.00646	0.00296	0.000331	0.00452	0.00942	0.00143	0.00384
La	0.0122	0.437	1.30	0.547	0.289	0.749	0.253	0.401	0.485
Ce	0.0353	0.881	3.79	1.09	0.815	1.85	0.598	1.03	0.700
Pr	0.00541	0.0855	0.469	0.0854	0.0744	0.211	0.0684	0.108	0.0558
Sr	0.230	11.0	21.6	6.22	4.62	14.8	3.32	7.53	10.3
Nd	0.0268	0.327	1.93	0.249	0.231	0.628	0.274	0.389	0.204
Sm	0.0137	0.0750	0.404	0.0402	0.0376	0.112	0.0619	0.0732	0.0745
Zr	0.270	1.81	6.04	0.323	0.0724	0.508	3.05	0.747	0.788
Hf	0.0206	0.0371	0.0592	0.00780	0.00731	0.0250	0.0295	0.0154	0.0308
Eu	0.00399	0.0257	0.129	0.0162	0.0171	0.0371	0.0150	0.0247	0.0281
Gd	0.0203	0.0969	0.334	0.0456	0.0568	0.0959	0.0588	0.0796	0.0975
Tb	0.00348	0.0147	0.0494	0.00799	0.0116	0.0206	0.00903	0.0119	0.0171
Dy	0.0258	0.112	0.298	0.0673	0.0961	0.0902	0.0728	0.0783	0.117
Ho	0.00631	0.0235	0.0587	0.0171	0.0242	0.0229	0.0209	0.0178	0.0276
Er	0.0223	0.0711	0.174	0.0575	0.0778	0.0595	0.0669	0.0562	0.0818
Yb	0.0342	0.0879	0.196	0.0774	0.0902	0.0686	0.0807	0.0725	0.0953
Lu	0.00789	0.0150	0.0344	0.0148	0.0194	0.0243	0.0154	0.0129	0.0159
Pb	0.0120	0.0536	0.0345	0.0258	0.0104	0.166	0.0219	0.0512	0.0277
Th	0.00110	0.0107	0.0575	0.0857	0.0118	0.0716	0.0211	0.0191	0.00735
U	0.000477	0.00449	0.0183	0.0292	0.00461	0.0441	0.00844	0.00713	0.00466